Title

Mitochondrial mRNA localization is governed by translation kinetics and spatial transport

Journal

PLOS Computational Biology, 18(8)

ISSN

1553-734X

Authors

Arceo, Ximena G
Koslover, Elena F
Zid, Brian M
et al.

Publication Date

2022

DOI

10.1371/journal.pcbi.1010413

Peer reviewed

PLOS COMPUTATIONAL BIOLOGY

RESEARCH ARTICLE

Mitochondrial mRNA localization is governed by translation kinetics and spatial transport

Ximena G. Arceo[1], Elena F. Koslover[2], Brian M. Zid[1]*, Aidan I. Brown[3]*

1 Department of Chemistry & Biochemistry, University of California, San Diego, La Jolla, California, United States of America, **2** Department of Physics, University of California, San Diego, La Jolla, California, United States of America, **3** Department of Physics, Ryerson University, Toronto, Canada

* zid@ucsd.edu (BMZ); aidan.brown@ryerson.ca (AIB)

Citation: Arceo XG, Koslover EF, Zid BM, Brown AI (2022) Mitochondrial mRNA localization is governed by translation kinetics and spatial transport. PLoS Comput Biol 18(8): e1010413. https://doi.org/10.1371/journal.pcbi.1010413

Editor: Jun Allard, University of California Irvine, UNITED STATES

Received: June 10, 2022

Accepted: July 19, 2022

Published: August 19, 2022

Peer Review History: PLOS recognizes the benefits of transparency in the peer review process; therefore, we enable the publication of all of the content of peer review and author responses alongside final, published articles. The editorial history of this article is available here: https://doi.org/10.1371/journal.pcbi.1010413

Data Availability Statement: Source code (in Matlab) for model simulation is available at: https://github.com/aidanbrowntmu/MitoMrnaLoc. Input data for simulations, output data from simulations,

Abstract

For many nuclear-encoded mitochondrial genes, mRNA localizes to the mitochondrial surface co-translationally, aided by the association of a mitochondrial targeting sequence (MTS) on the nascent peptide with the mitochondrial import complex. For a subset of these co-translationally localized mRNAs, their localization is dependent on the metabolic state of the cell, while others are constitutively localized. To explore the differences between these two mRNA types we developed a stochastic, quantitative model for MTS-mediated mRNA localization to mitochondria in yeast cells. This model includes translation, applying gene-specific kinetics derived from experimental data; and diffusion in the cytosol. Even though both mRNA types are co-translationally localized we found that the steady state number, or density, of ribosomes along an mRNA was insufficient to differentiate the two mRNA types. Instead, conditionally-localized mRNAs have faster translation kinetics which modulate localization in combination with changes to diffusive search kinetics across metabolic states. Our model also suggests that the MTS requires a maturation time to become competent to bind mitochondria. Our work indicates that yeast cells can regulate mRNA localization to mitochondria by controlling mitochondrial volume fraction (influencing diffusive search times) and gene translation kinetics (adjusting mRNA binding competence) without the need for mRNA-specific binding proteins. These results shed light on both global and gene-specific mechanisms that enable cells to alter mRNA localization in response to changing metabolic conditions.

Author summary

Mitochondria are important generators of adenosine triphosphate (ATP), the energy currency of the cell. In the brewer's yeast, Saccharomyces cerevisiae, cells can switch ATP generation towards or away from mitochondria depending on the environment. Understanding how cells carry out this switch of mitochondrial function may provide insight into the loss of mitochondrial function, a hallmark of many age-related diseases. Many mRNAs that encode mitochondrial proteins are synthesized in the nucleus, but become localized to the mitochondrial surface during protein production. While some of these

and Matlab files to create plots in figures are provided as a supplemental file.

Funding: AIB was supported by a Natural Sciences and Engineering Research Council of Canada (nserc-crsng.gc.ca/) Discovery Grant 2021-03431 and start-up funds provided by the Ryerson University Faculty of Science (https://www.torontomu.ca/science/). EFK was supported by NSF (nsg.gov) grant #2034482, and a Cottrell Scholar Award from the Research Corporation for Science Advancement (rescorp.org). BMZ was supported by NIH (nih.gov) grant R35GM128798. The funders had no role in study design, data collection and analysis, decision to publish, or preparation of the manuscript.

Competing interests: The authors have declared that no competing interests exist.

mRNAs always localize to the mitochondria, others do so only in response to certain food sources driving energy production. In this study we created a mathematical model of mRNA localization to the mitochondria to understand what factors differentiate these two mRNA classes. Our analysis implicates protein translation kinetics as well as the mitochondrial volume as the key factors that control whether mRNA localize to mitochondria. This work provides insight into how global alteration in mitochondrial content and gene-specific modulation of protein synthesis kinetics can couple together to adjust mRNA localization and potentially mitochondrial function.

Introduction

To sustain life and function, cells maintain a homeostatic internal state while retaining the capacity to respond to variable environments and challenges. For eukaryotic cells, homeostasis requires not only regulation of gene expression, but also maintainance of internal organization through the sorting of proteins among organelles and subcellular compartments. Spatial targeting of proteins to specific cellular destinations can occur through a variety of transport and retention mechanisms, sometimes acting in combination [1–7].

Protein localization is often controlled by first transporting the mRNA to a specific region [8], and then translating proteins locally. mRNA localization serves as a key mechanism for delivering proteins to far-flung cell regions in neurons [9], expediting protein synthesis when locally required [10], and ensuring proteins are provided a suitable environment for folding [11]. Failure to localize mRNA can result in developmental defects [12] and cognitive disorders [13].

Canonical descriptions of protein localization through mRNA transport include translational suppression en route [8, 14], with protein synthesis beginning only after the mRNA reaches its target destination. By contrast, some mRNA are known to begin translation while in transit [15, 16]. For such cases, we explore how translational dynamics themselves can control mRNA localization, focusing on nuclear-encoded mitochondrial genes in yeast.

While some mitochondrial genes are encoded by mitochondrial DNA, the vast majority of mitochondrial proteins are translated from nuclear-encoded mRNA [17] and a subset of those mRNAs have been observed to localize to the mitochondrial surface. In *Saccharomyces cerevisiae* these mitochondrially localized mRNAs have been subclassified based on their mechanism of localization. Class I mRNAs are primarily targeted to the mitochondria by the RNA binding protein Puf3, while Class II mRNAs localize independently of Puf3 [18, 19]. Class II mRNAs are proposed to localize through translation of the amino-terminal mitochondrial targeting sequence (MTS) that can associate with import complexes on the cytosolic side of the outer mitochondrial membrane [20].

S. cerevisiae yeast rely heavily on glucose fermentation even in aerobic conditions. With non-fermentable carbon sources, the shift to a respiratory metabolism involves dramatic changes to the mitochondrial proteome [21, 22]. This shift also leads to an increase in the fraction of the cytosol occupied by mitochondria (mitochondrial volume fraction, or MVF) [23], which form dynamic tubular networks distributed throughout the cell [24]. While Class II mRNAs were initially found to be mitochondrially localized under respiratory conditions, many exhibit condition-dependent localization, as almost 70% do not robustly localize to mitochondria under fermentative conditions [23, 25, 26]. This may be due at least in part to changes in MVF, which can quantitatively predict the conditional localization behavior of mRNAs *ATP2* and *ATP3* [23]. Additionally, many Class II mRNAs that do not robustly

localize under fermentative conditions, including *ATP2* and *ATP3*, become mitochondrially localized upon application of the translation elongation inhibitor cycloheximide (CHX) [23, 25]. By contrast, other Class II mRNAs such as *TIM50* have high, constitutive localization to mitochondria even in fermentative conditions [23], and respond little to increased MVF [23] or CHX application [25]. Given that all Class II mRNAs contain an MTS but only some are localized under fermentative conditions, these observations suggest that the presence of the MTS is required but not sufficient for preferential localization to mitochondria. This idea has been further supported through MTS swapping experiments [20].

Localization of a Class II mRNA to a mitochondrion requires exposure of an MTS peptide sequence while the mRNA is very near to the mitochondrial membrane, implying that such localization can be modulated through the relative kinetics of MTS exposure and spatial movement throughout the cell. By arresting translation, CHX leaves nascent peptides and any of their translated MTS motifs exposed indefinitely. The increase in mRNA localization upon CHX application thus substantiates the importance of gene-specific translation dynamics for mitochondrial localization. Similarly, the dependence of mitochondrial localization on the MVF suggests that the geometry encountered by a diffusing mRNA can meaningfully control the frequency of mitochondrial proximity and opportunities for an MTS to interact with a mitochondrial surface.

The physical process of localization requires a transport mechanism enabling an mRNA to encounter its target region and a retention mechanism to limit mRNA escape. In the relatively small volume of a yeast cell, diffusion is sufficient to distribute mRNA, with diffusive arrival rates to cellular targets modulated by intracellular geometry [7, 27–32]. Once an mRNA has diffusively reached a destination, binding interactions then determine the time period of mRNA localization. Equilibrium mRNA localization would be determined by the probability of occupying a binding-competent state and the volume of the localization region, i.e. the MVF. However, the energy-consuming process of translation pushes mRNA localization out of equilibrium, similar to other driven processes necessary to maintain cellular organization, including protein targeting [6, 7, 33–36].

To address how translational dynamics could control the localization of mRNA for mitochondrial genes, we developed a stochastic, quantitative model for mitochondrial mRNA localization that incorporates translation and diffusion within a yeast cell. The model is parameterized against published genome-wide measurements of both constitutively and conditionally localized Class II mRNAs [22, 37, 38]. We find that the kinetics of translation, as well as the diffusive search time-scales, determine the level of mRNA localization to mitochondria, enabling both low and high localization within the physiological range of key parameters. Crucial to our description of mitochondrial mRNA localization is a proposal for an MTS maturation time following translation of the MTS peptide sequence. Our work suggests a distinct mode of spatial protein regulation and a mechanism for yeast and other cells to control protein localization using gene-specific translation dynamics combined with global adjustments of organelle size.

Results

Localization depends on both equilibrium and kinetic contributions

To help guide our investigation of the translational control of mRNA localization, we begin by analyzing a general minimal model (Fig 1A). We assume that mRNA is capable of switching between a binding-competent ("sticky") state and a binding-incompetent ("non-sticky") state. For mitochondrial targeting, a binding-competent state corresponds to an mRNA with at least one partially-translated peptide with an exposed MTS sequence. We define two rate constants:

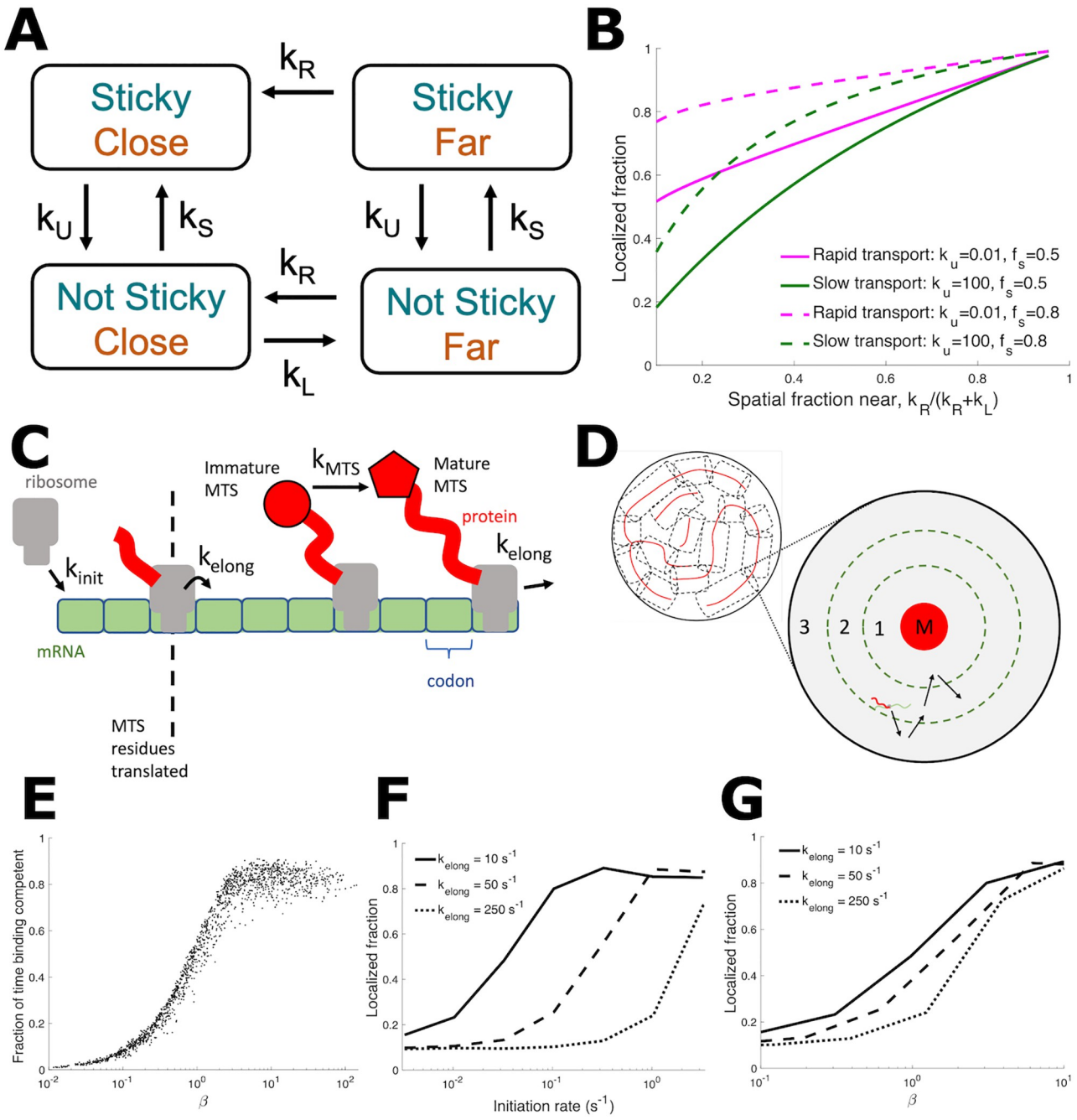

Fig 1. Quantitative models show equilibrium and kinetic contributions to mitochondrial mRNA localization. (A) Simplified discrete-state model of mRNA mitochondrial localization. mRNA can be either binding competent ('sticky') or not binding competent ('not sticky'), and either within binding range of mitochondria ('close') or not within binding range ('far'). mRNA transition between these states with rates described in the text. (B) Localized fraction [defined as 'close' in (A)] as the spatial fraction of the cell near mitochondria (Eq 2) is varied. Rapid transport curves indicate rapid switching from close to far relative to switching between sticky and not sticky, while for slow transport the relative switching speeds are reversed. (C) Stochastic model of mRNA translation. Ribosomes initiate translation at rate k_{init} and progress to the next codon at rate k_{elong}. MTS is translated after the first 100 amino acids. Once MTS is translated, MTS becomes binding-competent at rate k_{MTS}. (D) Schematic of mRNA diffusion in spatial model, shown in cross-section. The cytoplasmic space is treated as a cylinder centered on a mitochondrial cylinder (red): the three dimensional volume extends along the cylinder axis. mRNA in region 1 are sufficiently close for binding-competent mRNA to bind to the mitochondria, mRNA in region 2 are considered mitochondrially localized in diffraction-limited imaging data, and region 3 represents the remainder of the cell volume. mRNA not bound to mitochondria will freely diffuse between these regions. (E) For the stochastic translation model shown in (C), the fraction of mRNA lifetime that an mRNA is binding-competent vs. $\beta = k_{init}(L - L_{MTS})/k_{elong}$, the mean number of translated MTSs per mRNA. For each data point, mRNA translation parameters k_{init}, L, and k_{elong} were randomly selected from the ranges $k_{init} \in [10^{-3}\ s^{-1}, 0.5\ s^{-1}]$, $L \in [150\ aa, 600\ aa]$, and $k_{elong} \in [1\ s^{-1}, 10\ s^{-1}]$. (F) Mitochondrial localization from the stochastic model illustrated in C and D, as k_{init} is varied. $L = 400$ aa, 4% mitochondrial volume fraction, and k_{elong} as indicated in legend. (G) is the same data as F, but plotted against β.

https://doi.org/10.1371/journal.pcbi.1010413.g001

k_S and k_U for switching into and out of the competent state, respectively, assumed to be independent of the mRNA location. At equilibrium the fraction

$$f_s = \frac{k_S}{k_S + k_U} \tag{1}$$

is in the competent state. For a binding-competent mRNA to bind to a mitochondrion, it must be sufficiently proximal to a mitochondrial surface. Binding-incompetent molecules can move from the bulk into binding range of a mitochondrion with rate k_R and can leave the near-surface region with rate k_L. These rates are expected to depend on the diffusivity of the mRNA and the geometry (size and shape) of mitochondria within the cell. At equilibrium,

$$f_d = \frac{k_R}{k_R + k_L} \tag{2}$$

is the fraction of the mRNA-accessible cell volume that is within binding range of the mitochondrial surface. As the cytosolic volume fraction that is near mitochondria, f_d is distinct from but related to the MVF, the cell volume fraction occupied by mitochondria. The binding-competent mRNA reach the mitochondrial region with the same rate k_R but are assumed to bind irreversibly and cannot leave until they switch into the incompetent state.

The resulting four-state model (binding-competent vs not, proximal to mitochondria vs not) is illustrated in Fig 1A. Given the assumed irreversible binding of competent mRNAs, the model is inherently out of thermal equilibrium. The kinetic equations can be solved to find the steady-state fraction of mRNA localized to the proximal region, as a function of the kinetic rates (see Methods).

The solutions exhibit two limiting regimes of interest. In the rapid-transport regime where mRNA transport is much faster than the competence switching rate (k_U, $k_S \ll k_R$, k_L), incompetent mRNA can equilibrate throughout the entire cell prior to a switching event. Similarly, competent mRNA can rapidly reach the proximal region and bind to mitochondria. The fraction of mRNA that are mitochondrially localized is then given by the two equilibrium fractions,

$$f_{loc} = f_s + (1 - f_s) f_d \ . \tag{3}$$

In this spatially equilibrated situation, changing the mitochondrial volume fraction would affect only f_d. If binding dynamics are held fixed (fixed f_s), the mitochondrially localized fraction f_{loc} will depend linearly on the proximal volume fraction f_d, with the slope determined by the equilibrium binding competence f_s.

In the opposite slow-transport regime, mRNA transport is much slower than the switching rate (k_R, $k_L \ll k_U$, k_S) and the fraction localized is given by:

$$f_{loc} = \frac{1}{1 + (1 - f_s)(1 - f_d)/f_d} \ . \tag{4}$$

This regime exhibits nonequilibrium behavior. In the limit of low mitochondrial volume fraction ($f_d \ll 1$), the localization probability goes to zero. This is a fundamental difference from the rapid-transport regime, where even at low volume fractions, binding-competent mRNA localize to mitochondria. As a result, the regime with slow transport and fast switching is expected to exhibit a steeper, more non-linear increase in localization with increasing mitochondrial volume fraction (green lines in Fig 1B) compared to the rapid-transport regime (magenta lines in Fig 1B).

This highly simplified, analytically tractable, four-state model is agnostic to the mechanistic details for how the switching between binding-competent and incompetent states occurs, as well as the geometric details of diffusive transport to and from the mitochondria-proximal region. Specifically, it highlights some important non-intuitive features of localization for any molecule that can switch between competent and incompetent states. Namely, the localization behavior is expected to depend not just on the equilibrated binding-competent fraction f_s (Eq 1) and proximal fraction f_d (Eq 2) but also on the relative kinetics of spatial transport and competence switching. In the nonequilibrium regime of fast switching and slow transport, localization becomes non-linearly sensitive to the volume fraction of the target region.

For the mitochondrial localization of mRNA, the switching times between competent and incompetent states are determined by translation kinetics that control exposure duration for attached MTS peptide sequences. The transport kinetics are determined by diffusion timescales towards and away from the mitochondrial surface. We next proceed to develop a more mechanistically detailed model for mitochondrial localization that directly incorporates translation and diffusion.

Stochastic simulation incorporates translation and diffusive kinetics

The translation kinetics model (Fig 1C) tracks ribosome number and position. Ribosomes initiate translation on an mRNA with rate k_{init}, and then proceed along the mRNA codons at elongation rate k_{elong}. The mRNA is L codons in length. The number of codons that must be translated to complete the MTS is set to $l_{\text{MTS}} = 100$ to account for an MTS length of up to 70 amino acids and a ribosome exit tunnel length of $\sim$ 30 amino acids [39, 40]. We begin with an 'instantaneous' model, where once translation moves past l_{MTS}, the mRNA-ribosome complex is assumed to be binding competent until translation completes ($k_{\text{MTS}} \to \infty$ in Fig 1C). In subsequent sections we will consider alternative binding-competence models with finite k_{MTS}.

An mRNA can have multiple MTS-containing nascent peptides if a subsequent ribosome initiates and translates another MTS before the prior translation event is complete. The average number of such binding-competent peptides on a given mRNA is given by

$$\beta = \frac{k_{\text{init}}(L - l_{\text{MTS}})}{k_{\text{elong}}} \quad . \tag{5}$$

To describe the diffusive encounter of an mRNA with the mitochondrial network, we use a simplified geometric model appropriate for diffusive search towards a narrow tubular target. Specifically, we treat the geometry as a sequence of concentric cylinders, each representing an effective region surrounding a tubule of the mitochondrial network (Fig 1D). Fig 1D shows a two-dimensional cross-sectional view of this three-dimensional geometry. The innermost cylinder represents a mitochondrial tubule and serves as a reflective boundary for the mRNA. A slightly larger cylinder represents the region where a binding-competent mRNA is sufficiently close to bind to the mitochondrial surface. If one or more binding-competent MTSs are exposed on an mRNA when it reaches the vicinity of the innermost cylinder, the mRNA will remain associated to the mitochondrial surface until the mRNA returns to zero binding-competent MTSs after peptide translation is completed. A still wider cylindrical region represents locations where the transcript would appear close to the mitochondrial tube in diffraction-limited imaging data, but may not be sufficiently close to bind the mitochondrial surface. Finally, the outermost reflecting cylinder represents the cytoplasmic space available to the diffusing mRNA. The radius of this external cylinder is set such that the innermost mitochondrial cylinder encloses the correct volume fraction of mitochondria to correspond to experimental measurements (which can range from 1%–15%).

This simplified geometry gives an approximate description of the search process for the mitochondrial surface, based on the idea that whenever the mRNA wanders far from any given mitochondrial tubule it will approach another tubule in the network (Fig 1D), so that its movement can be treated as confinement within an effective reflecting cylinder. Such an approach has previously been used successfully to approximate the diffusive process of proteins searching for binding sites on long coils of DNA [31]. More detailed geometrical features, such as the specific junction distribution and confinement of the yeast mitochondrial network to the cell surface are neglected in favor of a maximally simple model that nevertheless incorporates the key parameters of mitochondrial volume fraction and approximate diffusive encounter time-scale.

Simulations of our stochastic model for simultaneous translation and diffusion can be carried out with any given set of gene-specific translation parameters (k_{init}, k_{elong}, L). The simulated mRNA trajectories are then analyzed to identify the fraction of mRNA found within the region proximal to the mitochondrial surface (see Methods for details). By exploring the physiological range of translation parameters, many orders of magnitude of the mean number of translated MTSs per mRNA (β, see Eq 5) are covered, which also covers the full range of mRNA binding competence (Fig 1E). We find that, for any set of physiological translation parameters, the number of binding-competent MTS sequences (β) is predictive of the fraction of time (f_s) that each mRNA spends in the binding competent state (Fig 1E). The greatest variation is near $\beta \approx 1$, where different parameter combinations with the same average number of exposed MTSs can give competency fractions ranging from $30 - 50\%$.

Our analytically tractable 4-state model (Fig 1B) indicates that localization fraction should depend not only on the binding competent fraction f_s (related to β) but also on the kinetics of switching between competent and incompetent states. We explore the effect of translation kinetics on localization in the stochastic model by varying the initiation and elongation rates of a fixed-length mRNA (Fig 1F). This approach samples the scope of localization behaviors by simulating multiple combinations of translation parameters. We include unphysiologically high elongation rates to compare to the expected behavior from the 4-state model. As expected, faster elongation rates (which decrease the period an MTS is exposed on an mRNA and decrease β) result in lower localization, and higher initiation rates (which increase β while leaving MTS exposure time unaffected) result in higher localization (Fig 1F). While the number of exposed MTSs, β, can explain much of the effect of changing elongation and initiation rates (Fig 1G), there is substantial variability in localization around $\beta \approx 1$, with faster elongation decreasing localization. This result is consistent with the prediction of the 4-state model that rapid switching of binding competence can lead to lower localization even for equal binding competent fractions f_s.

Physiological translation parameters lead to high mitochondrial binding competence and localization

Because translation kinetics and length vary between genes, we expect the kinetics of binding-competence switching and thus the mitochondrial localization to be gene-specific. To explore the relationship between translation kinetics and mitochondrial localization, we define two categories of Class II mRNAs that were all found to be localized in respiratory conditions [19] by their localization sensitivity to translation elongation inhibition by cycloheximide (CHX) in fermentative conditions [25]. "Constitutive" mRNAs preferentially localize to mitochondria both in the absence and presence of CHX. "Conditional" mRNAs do not preferentially localize to mitochondria in the absence of CHX, but do so following CHX application.

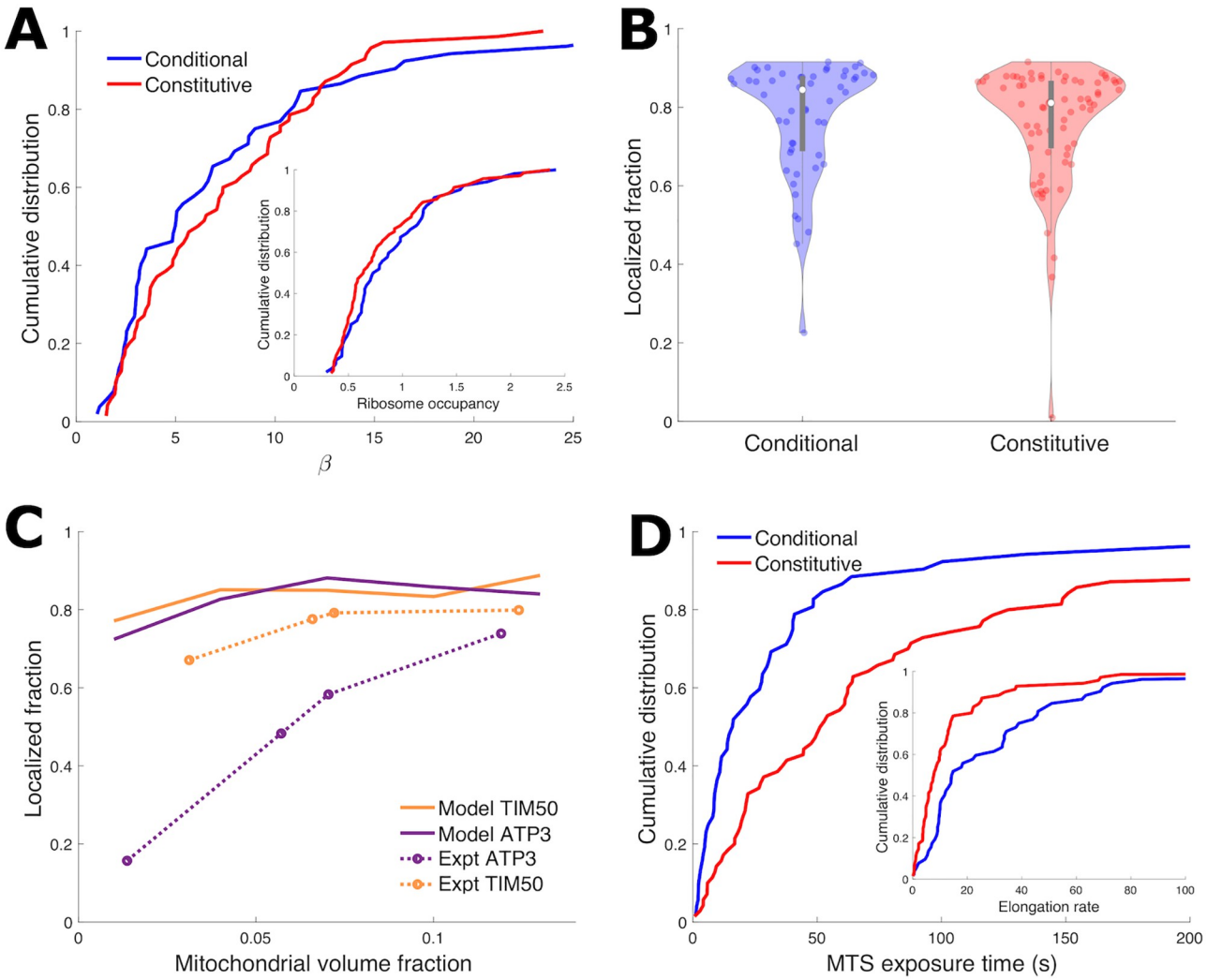

Fig 2. Instantaneous model is insufficient to explain differential mitochondrial localization of different gene groups. (A) Cumulative distributions of conditional and constitutive mRNA genes vs number of binding-competent ribosomes β (lines indicate fraction of genes with given β or less). β for each mRNA gene is calculated from gene-specific k_{init} and k_{elong} that are estimated from experimental data (see Methods). Inset is cumulative distribution of ribosome occupancy [38], showing ribosome occupancy and β have similar distributions. (B) Violin plot [41] showing mRNA localization fraction of individual genes with instantaneous model (no maturation delay), with translation kinetics for each gene estimated from experimental data (see Methods). 4% MVF. For direct comparison to experimental data, mRNA in region 1 (see Fig 1D) recorded as mitochondrially localized. (C) Mitochondrial localization vs mitochondrial volume fraction for *TIM50* and *ATP3* with instantaneous model (solid lines), with translation kinetics for both genes estimated from experimental data (see Methods). For direct comparison to experimental data (dotted lines with circles), mRNA in regions 1 and 2 (see Fig 1D) recorded as mitochondrially localized. (D) Cumulative distributions of MTS exposure time $t_{\text{expo}} = (L - l_{\text{MTS}})/k_{\text{elong}}$. The steeper rise of conditional genes indicates more conditional gene mRNAs have low exposure times. Translation kinetics for each gene estimated from experimental data (see Methods). Inset shows the cumulative distribution of elongation rate, for which constitutive genes have a steeper rise, indicating slower typical elongation, which contributes to the longer exposure times in the main plot.

https://doi.org/10.1371/journal.pcbi.1010413.g002

Using protein per mRNA and ribosome occupancy data [22, 37, 38, 42], we estimated the gene specific initiation rate k_{init} and elongation rate k_{elong} for 52 conditional and 70 constitutive genes (see Methods). Along with the known mRNA lengths L, these parameters quantitatively describe translation of each gene in the yeast transcriptome. These measurements [38] indicate that conditional and constitutive genes have similar distributions of ribosome occupancy (Fig 2A, inset; see S1 Fig for similar distributions of conditional and constitutive gene

ribosome occupancy derived from [43]). Conditional and constitutive genes also have similar distributions of the number of exposed MTSs, β, as calculated from estimated translation parameters (Fig 2A). Notably, the predicted β values were relatively large, with 90% of both constitutive and conditional mRNA estimated to have $\beta > 2$. Consequently, the stochastic simulation predicts median localization fractions above 80% for both the conditional and constitutive gene groups, with no significant difference between the two groups (Fig 2B). Comparison of two specific genes (*ATP3* and *TIM50*) known to have mitochondrial localizations with distinct dependence on mitochondrial volume fraction [23] also yielded similarly high localization fractions in stochastic simulations, across all mitochondrial volume fractions (Fig 2C).

These simulation results using gene-specific estimates of the translation parameters k_{init}, k_{elong}, and L (Fig 2B and 2C) run directly counter to experimental measurements. Specifically, they over-predict mitochondrial localization for transcripts, such as *ATP3*, that are known to exhibit low localization values at low mitochondrial volume fractions. Given the high calculated values of β, and the importance of MTS exposure kinetics in predicting localization at intermediate β values, we more closely examined the quantities underlying this parameter, which describes the number of exposed complete MTSs. We find that the distributions of both the elongation rate and the MTS exposure time $t_{\text{expo}} = (L - l_{\text{MTS}})/k_{\text{elong}}$ substantially differ between the two gene groups, with conditionally localized genes exhibiting more rapid elongation and shorter MTS exposure times (Fig 2D; see S2 Fig for similar distributions of conditional and constitutive gene elongation rates derived from [42]). These differences in MTS exposure kinetics between the two gene groups point towards a mechanism, thus far not part of our quantitative model, that would reduce the number of exposed MTSs (β), allowing for more variability in localization between the two groups. At the same time, this mechanism should have a greater effect in reducing MTS exposure time in conditionally localized genes, enabling reduced localization of this group at low mitochondrial volume fractions.

Mitochondrial binding competence requires a maturation period

To reduce β and MTS exposure time, we introduce into our quantitative model a time delay between complete translation of the MTS and maturation of the MTS signal to become binding competent (Fig 1C, $k_{\text{MTS}} < \infty$). This additional parameter is consistent with evidence that mitochondrially imported proteins require the recruitment of cytosolic chaperones to target them for recognition [44] and import by receptors on the mitochondrial surface [45–47]. During MTS maturation, which could include autonomous folding or interaction with additional chaperone proteins [48], the MTS becomes capable of binding the mitochondrial surface.

In the model, MTS maturation is treated as a stochastic process with constant rate k_{MTS} corresponding to an average maturation time $\tau_{\text{MTS}} = 1/k_{\text{MTS}}$. This maturation period decreases the binding-competent exposure time uniformly across all mRNA, and decreases the number of binding-competent MTS signals (i.e. lowers β) for all mRNA. The maturation period has the largest effect on short mRNAs with fast elongation, reducing their already short exposure times. Consequently, it is expected to have a larger effect on conditional versus constitutive genes.

The additional MTS maturation time does not alter the total time to translate an mRNA ($T_{\text{total}} = L/k_{\text{elong}}$). The ribosome continues elongating during maturation, and is located at a downstream codon when the MTS becomes binding competent. The mean steady-state

number of binding-competent MTSs per mRNA is

$$\beta_{\text{mature}} = \frac{k_{\text{init}}}{k_{\text{elong}}}\left\{L - l_{\text{MTS}} - \frac{k_{\text{elong}}}{k_{\text{MTS}}}\left[1 - \exp\left(-\frac{k_{\text{MTS}}}{k_{\text{elong}}}[L - l_{\text{MTS}}]\right)\right]\right\} . \quad (6)$$

The mean time that each MTS is binding competent is

$$t_{\text{expo,mature}} = (1 - e^{-k_{\text{MTS}}t})\left[\frac{1}{k_{\text{MTS}}}\frac{1 - e^{-k_{\text{MTS}}T_{\text{total}}}(k_{\text{MTS}}T_{\text{total}} + 1)}{1 - e^{-k_{\text{MTS}}T_{\text{total}}}}\right] . \quad (7)$$

For mRNA localization to be sensitive to mitochondrial volume fraction, we expect the MTS exposure time to be shorter than the diffusive search times at low MVF (slow search, long search time) and longer than diffusive search times at high MVF (fast search, short search time). Such an intermediate exposure time will allow for high mitochondrial localization exclusively at high MVF.

The mean search time for a particle of diffusivity D to find a smaller absorbing cylinder of radius r_1 when confined within a larger reflecting cylinder of radius $r_2 > r_1$ is [28]

$$t_{\text{search}} = \frac{1}{2D}\left[\frac{r_2^4}{r_2^2 - r_1^2}\log\left(\frac{r_2}{r_1}\right) - \frac{3r_2^2 - r_1^2}{4}\right] . \quad (8)$$

The smaller, absorbing radius r_1 represents the cylinder sufficiently close to bind the mitochondrial surface, while r_2 is the cylinder representing a typical distance that the diffusing particle must move through the cytoplasm to approach a different region of the mitochondrial network. As the mitochondrial volume fraction decreases, the radius r_2 and the diffusive search time to find the mitochondrial surface t_{search} both increase.

To understand the impact of MTS maturation, we consider a typical conditional and constitutive mRNA from each group, using median translation rates and gene length. Fig 3A shows the exposure time $t_{\text{expo,mature}}$ as the maturation time is varied. We find exposure times for a typical conditional gene to be intermediate between the high and low MVF diffusive search times when the maturation time is in the range τ_{MTS} = 10—100 seconds (Fig 3A). By contrast, the typical constitutive gene maintains an exposure time that is higher than the diffusive search time for this parameter range.

In addition to modulating the kinetics of binding competency, the maturation period decreases the expected number of functional MTS signals per mRNA, β (Fig 3B). For the typical conditional gene, β decreases to approximately 1 for maturation times of 40—50 seconds, while $\beta \approx 2.5$ for the typical constitutive gene in this range. The introduction of the MTS maturation time can thus selectively shift the expected number of functional MTS signals on conditional mRNA to the intermediate range ($\beta \approx 1$) necessary to allow for MVF sensitivity in the localization behavior. Under the same conditions, the constitutive mRNA would maintain a high number of functional MTSs and thus should remain localized even at low MVF.

Fig 3C shows how the localization for the prototypical conditional and constitutive mRNA varies with the maturation time. For very rapid MTS maturation ($\tau_{MTS} \to 0$), the MTS maturation model shows consistently high localization, as expected from the earlier model wherein the MTS became binding competent immediately upon translation. As the MTS maturation time increases and binding competency drops, both typical conditional and constitutive mRNA decrease their mitochondrial localization. However, the localization of the typical conditional mRNA begins to fall at approximately 10 seconds of maturation, while constitutive mRNA localization remains high until approximately 40 seconds of maturation. To provide a specific estimate of the maturation time, we determine the maturation times for which the

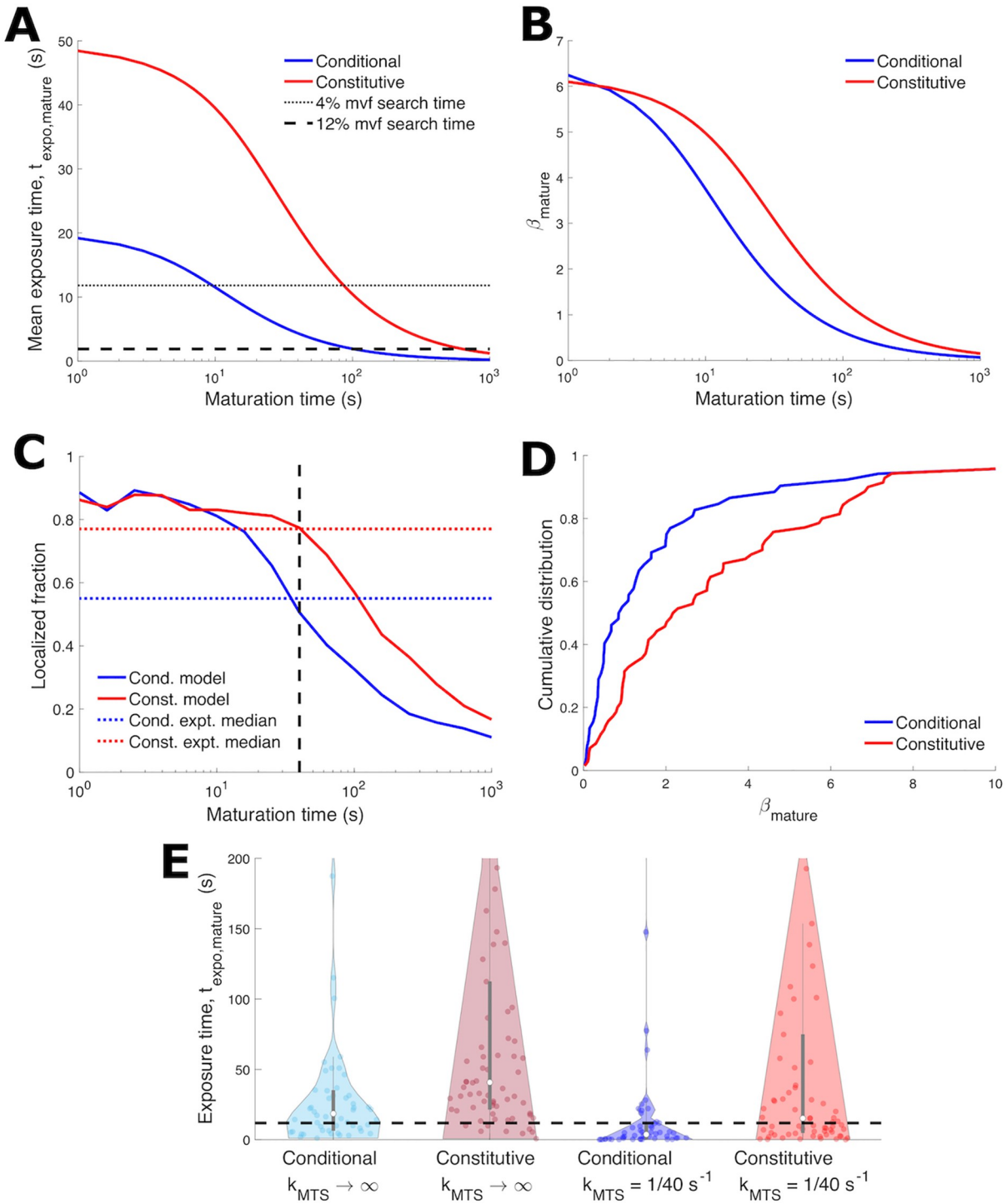

Fig 3. MTS binding-competence maturation time underlies distinct mitochondrial localization behavior of conditional and constitutive genes. (A) Mean exposure time of a binding-competent MTS before completing translation (Eq 7) vs binding-competence maturation time. Data for median conditional (L = 393 aa, k_{init} = 0.3253 s^{-1}, k_{elong} = 14.5086 s^{-1}) and constitutive genes (L = 483 aa, k_{init} = 0.1259 s^{-1}, k_{elong} = 7.7468 s^{-1}) is shown. Horizontal dashed lines are the mean diffusive search times (Eq 8) to reach binding range of mitochondria (region 1 in Fig 1D). (B) β_{mature} (mean number of mature binding-competent MTS signals, Eq 6) vs maturation time for median conditional and constitutive genes. (C) Mitochondrial localization (to region 1) vs maturation time for median conditional and constitutive genes with 4% MVF. Horizontal dotted lines indicate experimental localization medians. 40 second maturation time (vertical dashed line) allows model to match experimental localization for both conditional and constitutive genes. (D) Cumulative distribution of β_{mature} (mean mature MTS signals per mRNA) for conditional and constitutive genes. Steeper rise of conditional genes indicates more conditional genes have low β than

constitutive genes; compare to Fig 2A, which lacked MTS maturation time. (E) Violin plot showing model exposure times with 40-second MTS maturation and the instantaneous model without MTS maturation ($k_{MTS} \to \infty$). 4% MVF. Median conditional exposure time with maturation is below the diffusive search time to find the binding region (horizontal dashed line, Eq 8 for 4% MVF) while the other three medians are above this search time. For (C)—(E), the translation kinetics for each gene are estimated from experimental data (see Methods).

https://doi.org/10.1371/journal.pcbi.1010413.g003

model predicts the median experimental localization for conditional and constitutive genes (Fig 3C, intersection of dotted lines and solid lines). A single value of $\tau_{MTS} \approx 40$ seconds yields a simultaneous accurate prediction for the localization of both groups (Fig 3C, dashed).

Overall, the experimental data is consistent with a single gene-independent time-scale for MTS maturation. The stochastic model with a 40-second MTS maturation period was next applied to each of the conditional and constitutive mRNAs, for which translation parameters were calculated individually. With this maturation time, β_{mature} is substantially lower for conditional mRNA in comparison to constitutive mRNA (Fig 3D).

For conditional mRNAs without the maturation period ($k_{MTS} \to \infty$), the median MTS exposure time is greater than the diffusive search time (Fig 3E, dashed black line). With a maturation time of $\tau_{MTS} = 40$ s, the median conditional MTS exposure time decreases to be faster than diffusive search (Fig 3E). In contrast, constitutive mRNAs retained a median MTS exposure time longer than the diffusive search time, both with and without the 40-second maturation period.

Mitochondrial localization of conditional mRNAs is sensitive to inhibition of translational elongation and to mitochondrial volume fraction

Using the stochastic model with a 40-second MTS maturation period, we compute the localization of individual mRNAs in the constitutive and conditional groups, at a low mitochondrial volume fraction of 4%. Unlike the instantaneous model (with no MTS maturation delay), the localization of conditional genes is predicted to be significantly lower than that of constitutive genes (Fig 4A). While introduction of this maturation time distinguishes the mitochondrial localization of conditional and constitutive gene groups (Figs 4A vs 2B), changes to diffusivity are unable to separate the two gene groups (S3 Fig).

Furthermore, we use our model to predict localization in the presence of cycloheximide (CHX), which halts translation [49]. The localization difference in response to CHX application was used originally to define the constitutive and conditional groups [25]. The effect of CHX is incorporated in the model by assuming that all mRNAs with an exposed MTS at the time of CHX application will be able to localize to the mitochondrial surface, since further translation will be halted by CHX. We therefore compute from our simulations the fraction of mRNAs that have at least one fully translated (but not necessarily mature) MTS, defining this as the localization fraction in the presence of CHX. The model predicts that conditional genes will have a substantial difference in localization upon application of CHX, while the difference for localization of constitutive genes will typically be much smaller (Fig 4B). Qualitatively, this effect is similar to the observed difference in localization for experimental measurements with and without CHX (Fig 4C).

The predicted mitochondrial localization of the two example mRNAs, *ATP3* and *TIM50*, is shown in Fig 4D as a function of mitochondrial volume fraction. The model predicts *ATP3* localization is strongly sensitive to MVF, switching from below 30% at low MVF to above 70% localization at high MVF. By contrast, high localization of *TIM50* is predicted regardless of the MVF. The sensitivity of *ATP3* and insensitivity of *TIM50* localization to the MVF is consistent with experimental measurements indicating that *ATP3* exhibits switch-like localization under different metabolic conditions, while *TIM50* remains constitutively localized [23] (Fig 4D,

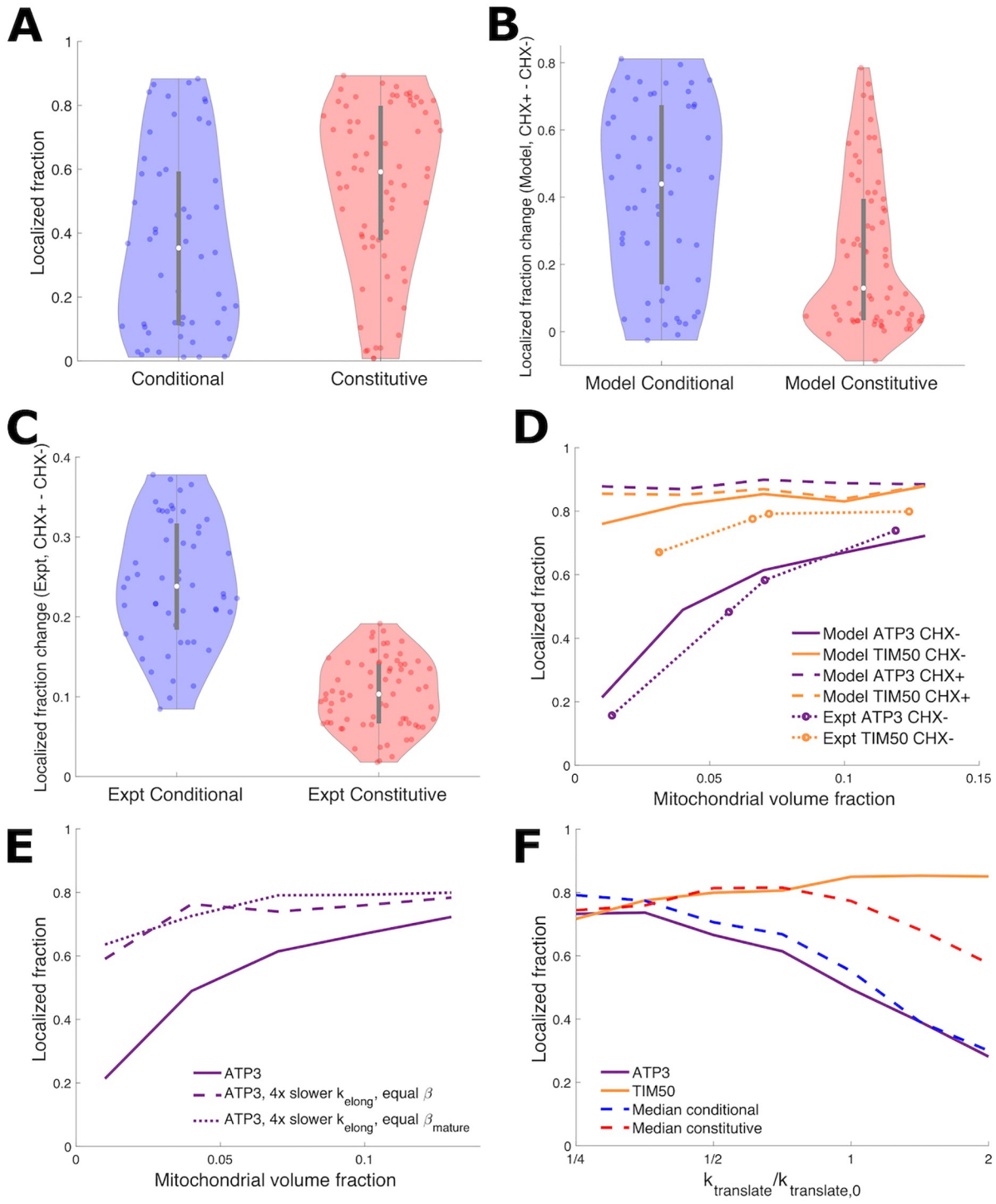

Fig 4. MTS maturation time distinguishes mRNA localization of conditional and constitutive genes. (A) Violin plots of mitochondrial localization of conditional and constitutive genes for model with 40-second maturation time; compare to Fig 2B, which lacked MTS maturation time. p-value = 0.5% for two-sample Kolmogorov-Smirnov test for a difference between conditional and constitutive localization distributions. (B,C) Violin plots of localization increase upon cycloheximide application for model with 40-second MTS maturation time (B) and from experiment (C). (D) Mitochondrial localization for *ATP3* and *TIM50* vs MVF for model with 40-second MTS maturation time. Solid lines are CHX-, which closely corresponds to experimental data [23] shown with dotted lines with circles. Dashed lines are CHX + model predictions, exhibiting large increase upon CHX application for *ATP3* and limited increase for *TIM50*. (E) Comparing model mitochondrial localization results for *ATP3* to similar hypothetical construct gene with decreased elongation rate and initial rate selected to maintain either MTS number β or mature MTS number β_{mature}. (F) Comparing model mitochondrial localization results for median

conditional and constitutive genes, *ATP3*, and *TIM50* as both elongation and initiation rates ($k_{translate}$) are varied. $k_{translate,0}$ is the elongation or initiation rate for each of *ATP3*, *TIM50*, and median conditional and constitutive genes. For all panels, the translation kinetics for each gene are estimated from experimental data (see Methods). For (F), see Fig 3 for median conditional and constitutive translation kinetics. (A), (B), and (F) use 4% MVF.

https://doi.org/10.1371/journal.pcbi.1010413.g004

dotted lines with circles). Dashed lines in Fig 4D show the predicted localization after CHX application, highlighting the difference in response to CHX between *ATP3* and *TIM50*.

The introduction of a delay period for MTS maturation both reduces the average number of binding-competent MTSs on each mRNA (lower β) and decreases the exposure time of each MTS. The latter effect results in faster switching between binding-competent and incompetent states for an mRNA. In the basic 4-state model, we saw that a steep sensitivity to the spatial region available for binding depends on having relatively rapid binding-state switching kinetics compared to the diffusion timescale (Fig 1B). As shown in Fig 3, the exposure time for conditional mRNAs is intermediate between the diffusive search times at high and low mitochondrial volume fractions. We therefore expect that the high rate of losing binding competence associated with the limited MTS exposure time to be critical for the switch-like response to mitochondrial volume fraction by *ATP3*.

As initiation rate can compensate for slowing translation elongation rates to maintain ribosome density [50, 51], we consider hypothetical constructs which have the same average ribosome density (equal β) or mature MTS number (β_{mature}) as *ATP3*, but 4-fold slower translational elongation rates. This results in slower switching kinetics, causing high localization and a loss of sensitivity to mitochondrial volume fraction (Fig 4E). We also consider how translation rate adjustment could control mRNA localization while remaining at a fermentative mitochondrial volume fraction (4%). Localization substantially decreases with increasing elongation and initiation rates for the median conditional gene and *ATP3*, while localization is less responsive to increased translation rates for the median constitutive gene and *TIM50* (Fig 4F). For responsive genes, translation rate modulation can adjust localization in a similar manner to mitochondrial volume fraction, with the potential for targeting of specific genes.

Overall, these results highlight the importance of translation kinetics, including both elongation rates and the maturation time of the MTS, in determining the ability of transcripts to localize to the mitochondrial surface. These kinetic parameters determine not only the equilibrated fraction of mRNAs that host a mature MTS but also the rate at which each mRNA switches between binding-competent and incompetent states. In order to achieve switch-like localization that varies with the mitochondrial volume fraction or CHX application, a transcript must exhibit an average of approximately one binding-competent MTS, with an exposure time that is intermediate between diffusive search times at low and high MVFs.

Discussion

We have investigated, using quantitative physical modeling and analysis of yeast transcriptome data, the role of translation kinetics in controlling MTS-mediated localization of nuclear-encoded mRNA to mitochondria. Specifically, we explored how mRNA binding competence and association with the mitochondrial surface, across a range of cellular conditions, is governed by the interplay of timescales for translation and cytoplasmic diffusion. We compared two sets of mRNA: one that is localized conditionally, when mitochondrial volume is expanded or when translational elongation is halted by cycloheximide, and another that localizes constitutively regardless of these conditions. For these 52 conditional and 70 constutitive mRNA we estimated gene-specific translation kinetics to apply in the model. Our analysis indicates that these two sets of transcripts exhibit global differences in translation kinetics, and

that these differences control mRNA localization to mitochondria by adjusting the number and duration of exposure for mitochondrial targeting sequences (MTSs) that are competent to bind to the mitochondrial surface.

It has previously been noticed when comparing mitochondrially localized versus non-localized yeast mRNAs, that localized mRNAs have features that reduce translation initiation and lower ribosome occupancy [52]. This observation seemed counterintuitive as MTS exposure was thought to be important for the localization of many of these mRNAs and hence higher ribosome occupancy would be expected to enhance localization by increasing the number of exposed MTSs [25, 53]. Lower occupancy was proposed to drive mRNA localization through increased mRNA mobility of a poorly loaded mRNA [52], as more mobile mRNA could more quickly find mitochondria when binding competent, increasing the localization of these mRNA. By contrast, our results imply an alternate prediction—that translational kinetics lead to enhanced localization of longer mRNAs, due to the increased number of loaded ribosomes bearing a binding-competent MTS. Indeed, constitutively localized mRNAs are on average longer than conditionally localized mRNAs. We show that translational parameters which yield a moderate number of approximately 1—2 binding competent ribosomes (via associated MTSs) per mRNA nevertheless allow robust localization under physiological conditions. Furthermore, this model occupancy allows for localization levels to be steeply sensitive to mitochondrial volume fraction, enabling transcript localization to be modulated by the MVF during changes to nutrient conditions and the metabolic mode. By constrast, transcripts with a high occupancy are expected to remain constitutively localized to mitochondria, regardless of the metabolic state of the cell. Thus, tuning of translational kinetics allows for differential response of transcript localization under varying nutrient conditions without the need for additional signaling pathways.

Translation kinetics can widely vary between genes, with greater than 100-fold variation in mRNA translation initiation rates and approximately 20-fold variation of elongation rates in yeast [42]. Translation duration can be further impacted by the length of the coding sequence. Constitutively localized mRNAs are on average longer and have slower translation elongation than conditionally localized mRNAs. Experimentally testing our proposal for translation-controlled localization would involve using combined mRNA and live translational imaging (as yet undeveloped in yeast), to directly measure translation and correlate localization with a time delay, presenting a fruitful pathway for future study. Cis regulators of translation elongation rates include mRNA features such as codon usage, codon context, and secondary structures [54, 55]. For the constitutively localized mRNA *TIM50* it was previously found that a stretch of proline residues, which are known to slow ribosome elongation, were necessary to maximize mRNA localization of this mRNA to the mitochondria [23].

To investigate the role of these varied parameters, we first explore an abstracted four-state model, wherein each transcript can be near or far from the mitochondrial surface and competent or not for binding to the mitochondria. This model shows that increasing the equilibrium fraction of time in the binding-competent state is indeed expected to enhance mitochondrial localization. Furthermore, the simplified model demonstrates that in order for transcript localization to be sensitive to the fraction of space where binding is possible (i.e., the mitochondrial volume fraction), the kinetics of switching in and out of the binding-compentent state must be relatively rapid compared to the kinetics for spatial movement.

We then proceed to develop a more detailed model that explicitly incorporates translational initiation and elongation, the formation of an MTS that enables mitochondrial binding, and diffusive search for the mitochondrial surface. This model confirms that tuning of the translation parameters can substantially alter mitochondrial localization, but only in a regime where the ribosome occupancy of the transcripts is relatively low. Surprisingly, plugging

physiological parameters into this instantaneous model resulted in the prediction that all mRNA transcripts studied would be highly localized to mitochondria in all conditions. In other words, the physiological parameters appeared to be in a regime where most transcripts had multiple binding-competent MTS sequences with long exposure time, resulting in global localization.

Motivated by differences in transcript length and elongation rate between constitutive and conditional gene groups, we incorporated an MTS maturation period into the model, driving the system into a parameter regime with lower numbers of binding-competent MTSs and shorter MTS exposure times, particularly for the more rapidly elongating and shorter conditional transcripts. Although we are unable to directly attribute this maturation period to a particular process, it aligns with other observations related to mitochondrial protein import. It is known that mitochondria targeting sequences mediate interactions with mitochondrial recognition machinery, namely TOM22 and TOM20 subunits of the translocase of the outer membrane (TOM) complex, and are necessary for efficient protein import into the mitochondria [56]. The folding process for some proteins that must be recognized and imported into mitochondria occurs on a timescale that competes with translocation [57, 58]. Furthermore, the formation of a secondary structure has been shown to be required for import of MTS-bearing proteins into mitochondria [59]. Together, these observations suggest the MTS is likely to require time to mature prior to becoming fully competent. Slowed translation has been suggested as providing an opportunity for proteins to fold, implying the MTS maturation time may also be regulated by translation kinetics [60].

In addition, molecular chaperones such as Hsp70 and Hsp90 are important for the delivery and recognition of the mitochondrial preproteins to the Tom70 receptor [46, 61]. Hsp70 expression levels have been found to have a direct effect on mRNA localization to the mitochondria [62]. STI1 is another cochaperone of Hsp70 and Hsp90 chaperones that plays a role in recognizing mitochondrial preproteins and mediates targeting to the mitochondria [47]. While the diffusive search for a newly-synthesized MTS by chaperones is expected be very fast ($\ll$40 s), chaperone- and co-chaperone-mediated folding can occur on timescales comparable to 40 seconds, including approximately tens of seconds in bacterial homologs [63, 64] and $>$ 100 seconds for human chaperone-mediated folding [65]. All of these data point to the need for a delay time between MTS translation and its maturation into a binding-competent state, via either autonomous folding or association with a chaperone, before it can be optimally recognized by the surface of the mitochondria.

Upon incorporation of a uniform (gene-independent) 40-second MTS maturation time into the model, we found that many genes fell into a parameter regime with only a few mature, binding-competent MTS sequences per transcript, and with intermediate exposure times for those sequences. This single choice of the maturation time made it possible to simultaneously match the expected localization of prototypical constructs representing both the constitutive and conditional gene groups. This choice of parameter yielded a mature MTS exposure time in the conditional gene that was longer than the diffusive search time at high mitochondrial volume fraction, yet shorter than the search time at low volume fraction. Consequently, the model with an MTS maturation time could adequately predict the decreased localization of conditional genes under metabolic conditions with low MVF, while genes in the constitutive group were localized regardless of the MVF. Previous experimental work suggested that changing mitochondrial volume fraction could control mitochondrial mRNA localization [23]—our quantitative modeling work provides further support for this mechanism of regulating mRNA localization.

Notably, conditional localization in our model required not only a modest number of mature MTS per transcript ($\beta_{\text{mature}} \approx 1$) but also relatively fast translational initiation and

elongation kinetics (short exposure times compared to diffusive search). This result demonstrates the out-of-equilibrium nature of the localization process, wherein localization is dictated by the kinetic rates themselves rather than their ratios or the equilibrated fraction of transcripts in different states. This feature arises due to broken detailed balance [66] in the kinetic scheme illustrated in Fig 1A, wherein binding-competent transcripts bind irreversibly to the mitochondrial surface and can be dislodged only by the completion of the energy-consuming translation process. Subcellular localization of mRNA can thus be added to the extensive list of biomolecular processes wherein the tools of non-equilibrium statistical mechanics elucidate the relevant physical parameters governing system behavior [6, 7, 33–36].

While we have focused on how variation in translational kinetics between genes can impact mitochondrial mRNA localization, there is also significant variation in mRNA decay timescales [67, 68]. Our model suggests (see S4 Fig) that the mRNA decay timescale has a limited effect on mitochondrial mRNA localization, unless the decay time is sufficiently short to compete with the timescale for a newly-synthesized mRNA to first gain binding competence. We leave specific factors thought to modulate mRNA decay, such as ribosome stalling [69], as a topic of future study.

In this work our quantitative model assumed uniform ribosome elongation rates along mRNA transcripts. In the presence of ribosome interactions, such dynamics can lead to both uniform and non-uniform ribosome densities and effective elongation rates along the transcript [70, 71]. With these uniform ribosome elongation rates, previous theoretical results suggest that collisions will be rare [70, 71]. However, elongation may not be homogeneous along an mRNA transcript, due to factors such as tRNA availability [72], boundaries between protein regions [73], amino acid charge [74], and short peptide sequences related to ribosome stalling [75]. We have found that slow (homogeneous) elongation facilitates mitochondrial mRNA localization, by providing time for MTS maturation, diffusive search, and to maintain binding-competent MTS-mediated mRNA binding to mitochondria. We expect that inhomogeneities in elongation rate along mRNA could either enhance or reduce mitochondrial mRNA localization, controlled by whether slower elongation is in regions that favor longer MTS exposure. For example, a ribosome stall site following full MTS translation could provide more time for MTS maturation and facilitate mitochondrial localization. Future experimental work could identify such stalling sequences and point towards how modeling can improve understanding of sequence impact on localization.

From the perspective of biological function, it remains unclear why some mitochondrial mRNAs localize conditionally under different metabolic conditions, while others remain constitutively localized. Both types contain an MTS [25, 76] and code for proteins rich in hydrophobic residues that are susceptible to misfolding and aggregation in the cytosolic space [44]. One reason for the differential localization may center on the altered function of mitochondria from fermentative to respiratory conditions. ATP synthase, the linchpin of the mitochondrial OXPHOS metabolic process, is comprised of subunits of both prokaryotic and eukaryotic origin [77]. Interestingly, all but one of the prokaryotic-origin subunits are conditionally localized to the mitochondria [23]. As mitochondrial mRNA localization has been found to be sufficient to upregulate protein synthesis [23, 78] we posit that conditional or switch-like localization behavior is a post-transcriptional regulation mechanism of protein synthesis that is sensitive to mitochondrial growth and metabolic state. In particular, this mechanism can act globally, altering expression levels for a large set of transcripts, even without the involvement for specific signaling pathways to adjust protein synthesis in response to metabolic state.

Furthermore, we propose that the effects of a respiratory metabolic state, which increases mitochondrial volume fraction and decreases the mRNA diffusion search time, can be mimicked through global translation elongation inhibition by pushing MTS signal dynamics into a

much slower regime than mRNA diffusive search, potentially altering mitochondrial composition. This hints at translation elongation inhibition as an avenue or tool for toggling metabolic modes within the cell. Similar means of post-transcriptional regulation may take place in mammalian cells as genome-wide mRNA localization measurements to the mitochondria have found a class of mRNAs that are constitutively localized while others are found to become localized after CHX administration [79].

Our results link the nonequlibrium physics governing localization of transiently binding-competent mRNA and the observed differential response of transcript groups that localize to mitochondria under varying metabolic conditions. The general principles established here, including the importance of translation kinetics and transport timescales to the organelle surface, apply broadly to cellular systems that rely on a peptide targeting sequence for co-translational localization of proteins. For example the localization of mRNAs encoding secretory proteins to the surface of the endoplasmic reticulum (ER) through interactions between the signal recognition sequence on the nascent peptide, the signal recognition particle that binds it, and receptors on the ER surface, may well be governed by analogous principles [80, 81]. By coupling together quantitative physical models and analysis of measured translational parameters for the yeast transcriptome, this work provides general insight on the mechanisms by which a cell regulates co-translational localization of proteins to their target organelles.

Methods

Simplified discrete-state model

Fig 1A describes a minimal model for mRNA localization with four discrete states: sticky and close (S_N), sticky and far (S_F), not sticky and close (U_N), and not sticky and far (U_F). mRNA can transition between these states with rates k_R, k_L, k_U, and k_S, as shown in Fig 1A. These transitions are mathematically described by

$$\frac{dS_N}{dt} = k_S U_N + k_R S_F - k_U S_N \ , \tag{9a}$$

$$\frac{dS_F}{dt} = k_S U_F - (k_U + k_R) S_F \ , \tag{9b}$$

$$\frac{dU_N}{dt} = k_U S_N + k_R U_F - (k_S + k_L) U_N \ , \tag{9c}$$

$$\frac{dU_F}{dt} = k_U S_F + k_L U_N - (k_S + k_R) U_F \ . \tag{9d}$$

Note that there is no direct transition from S_N to S_F because if an mRNA is bound to the mitochondria it cannot leave the mitochondrial vicinity. Setting all derivatives in Eq 9 to zero, the

steady-state solution is

$$\hat{S}_{\mathrm{N}} = \frac{1}{Z}\frac{k_{\mathrm{R}}k_{\mathrm{S}}(k_{\mathrm{L}}+k_{\mathrm{R}}+k_{\mathrm{S}}+k_{\mathrm{U}})}{k_{\mathrm{L}}k_{\mathrm{U}}(k_{\mathrm{R}}+k_{\mathrm{U}})} \ , \tag{10a}$$

$$\hat{S}_{\mathrm{F}} = \frac{1}{Z}\frac{k_{\mathrm{S}}}{k_{\mathrm{R}}+k_{\mathrm{U}}} \ , \tag{10b}$$

$$\hat{U}_{\mathrm{N}} = \frac{1}{Z}\frac{k_{\mathrm{R}}(k_{\mathrm{R}}+k_{\mathrm{S}}+k_{\mathrm{U}})}{k_{\mathrm{L}}(k_{\mathrm{R}}+k_{\mathrm{U}})} \ , \tag{10c}$$

$$\hat{U}_{\mathrm{F}} = \frac{1}{Z} \ , \tag{10d}$$

with

$$Z = \frac{(k_{\mathrm{S}}+k_{\mathrm{U}})[k_{\mathrm{L}}(k_{\mathrm{R}}+k_{\mathrm{U}})+k_{\mathrm{R}}(k_{\mathrm{R}}+k_{\mathrm{S}}+k_{\mathrm{U}})]}{k_{\mathrm{U}}k_{\mathrm{L}}(k_{\mathrm{U}}+k_{\mathrm{R}})} \ , \tag{11}$$

for state probabilities $\hat{S}_{\mathrm{N}} + \hat{S}_{\mathrm{F}} + \hat{U}_{\mathrm{N}} + \hat{U}_{\mathrm{F}} = 1$.

In the regime where mRNA transport is much faster than the binding-competence switching rate ($k_{\mathrm{R}}, k_{\mathrm{L}} \gg k_{\mathrm{U}}, k_{\mathrm{S}}$), the near fraction is

$$P_{\mathrm{N}} = \hat{S}_{\mathrm{N}} + \hat{U}_{\mathrm{N}} \simeq f_{\mathrm{s}} + (1-f_{\mathrm{s}})f_{\mathrm{d}} \ , \tag{12}$$

where $f_{\mathrm{s}} = k_{\mathrm{S}}/(k_{\mathrm{S}}+ k_{\mathrm{U}})$ and $f_{\mathrm{d}} = k_{\mathrm{R}}/(k_{\mathrm{R}}+ k_{\mathrm{L}})$. In the opposite regime, where mRNA transport is much slower than the binding-competence switching rate ($k_{\mathrm{R}}, k_{\mathrm{L}} \ll k_{\mathrm{U}}, k_{\mathrm{S}}$), the near fraction is

$$P_{\mathrm{N}} \simeq \frac{1}{1+(1-f_{\mathrm{s}})(1-f_{\mathrm{d}})/f_{\mathrm{d}}} \ . \tag{13}$$

Stochastic simulation with translation and diffusion

We use stochastic simulations to determine mitochondrial mRNA localization and fraction of time spent in the binding-competent state. Individual (non-interacting) mRNA molecules are simulated from synthesis in the nucleus to decay in the cytosol.

mRNA synthesis, translation, and MTS binding competence. The mRNA simulation begins after exit from the nucleus, as experiments can fluorescently label and track mRNA once synthesized in the nucleus. The time spent by mRNA in the nucleus is a normally-distributed time period with mean 60 s and standard deviation of 30 seconds (if a negative time is selected, the distribution is resampled until a positive time is yielded). After nuclear exit, the mRNA begins simulated translation and diffusion through the cytosol.

Each mRNA has L codons. Ribosomes arrive and initiate translation with rate k_{init} if the first codon is not occupied. Each ribosome on an mRNA moves forward to the next codon at rate k_{elong} if the next codon is not occupied. A ribosome on the L'th (final) codon completes translation at rate k_{elong}, leaving the final codon unoccupied. mRNA decay at a rate k_{decay} once in the cytosol. The parameters k_{init}, k_{elong}, and L are varied to represent different genes (see below for the calculation of k_{init} and k_{elong} for particular genes). The mRNA decay rate is set to $k_{\mathrm{decay}} = 0.0017\ \mathrm{s}^{-1}$ per mRNA molecule, such that the typical decay time for an mRNA molecule is 600 s. This decay time is consistent with measured average yeast mRNA decay times

ranging from 4.8 minutes [68] to 22 minutes [67]. Stochastic translation trajectories are generated using the Gillespie algorithm [82, 83].

We applied two models of mRNA gaining mitochondrial binding competence through mitochondrial targeting sequence (MTS) translation. For the instantaneous model, mRNA are competent to bind mitochondria if there is a least one ribosome at or past codon $l_{\mathrm{MTS}} = 100$. For the maturation model, once a ribosome reaches $l_{\mathrm{MTS}} = 100$, the ribosome will gain competence to bind the mRNA to a mitochodrion at a rate k_{MTS}. This rate k_{MTS} is included in the Gillespie algorithm, to select when a ribosome will confer binding competence.

Diffusion. The cell volume is defined as concentric cylinders. Fig 1D shows a two-dimensional cross-sectional view of this three-dimensional geometry: the volume extends along the cylinder axis. The central cylinder is the mitochondria, which is maintained at a radius $r_{\mathrm{m}} = 350$ nm. The radius R of the outer cylinder is selected to establish a desired mitochondrial volume fraction. A typical yeast cell volume is $V = 42\ \mu\mathrm{m}^3$. We assume that 80% of this volume is not occupied by the nucleus and vacuole, and thus available to mitochondria, the cytosol, and other cell components. Thus, the mitochondrial volume fraction in the simulation (r_{m}^2/R^2) is set equal to $f_m/0.8$ where f_m is the reported volume fraction. Specifically, we set $R = r_{\mathrm{m}}/\sqrt{f_{\mathrm{m}}/0.8}$. We note that this outer radius represents not the size of the cell as a whole, but rather the typical separation between non-proximal tubes within the mitochondrial network. A particle that hits the boundary of this outer cylinder would then begin to approach either the same or another mitochondrial network tube (see Fig 1D). We thus treat the outer cylinder as a reflecting boundary.

The simulation uses a propagator approach to sample the transitions of the mRNA between concentric regions around the mitochondrion, analogous to previous approaches used to simulate the dynamics of DNA-binding proteins [31] and diffusing organelles [84]. The closest region (region 1), for radial distances $r_{\mathrm{m}} < r < r_a = r_{\mathrm{m}} + 25$ nm, is sufficiently close for a binding-competent mRNA to bind a mitochondrion. mRNA within the intermediate cylindrical shell (region 2), with $r_a < r < r_b = r_{\mathrm{m}} + 250$ nm, are sufficiently close to the mitochondrion that they appear close in diffraction-limited imaging but are not sufficiently close to be able to bind. The last cylindrical shell (region 3), for $r_b < r < R$, represents the cell region where an mRNA would not be near any mitochondria.

We estimate the 25-nm binding distance by combining several contributions. The yeast ribosome has a radius of 13—14 nm [85]. The MTS region, up to 70 amino acids long, forms an amphipathic helix [39], a form of alpha helix. With an alpha helical pitch of 0.54 nm and 3.6 amino acids per turn, a 31 amino acid MTS (the mean of 20 yeast MTS lengths [86]) is approximately 5 nm in length. An additional few nanometers of other peptide regions bridging the MTS to the ribosome provides an estimate of 25 nm for the range of an MTS-bearing mRNA to bind mitochondria. The 250-nm imaging distance is based on the Abbe limit to resolution with visible light [87].

In the simulations, region 1 is treated as a cylinder with an absorbing boundary at $r_a + \epsilon$. A particle that first enters the region is placed at initial position $r_a - \epsilon$ and the first passage time to the absorbing boundary is sampled from the appropriate Green's function for radially symmetric diffusion in a cylindrical domain [88]. Region 2 is treated as a hollow cylinder with absorbing boundaries at $r_a - \epsilon$ and $r_b + \epsilon$. Particles that enter region 2 from region 1 start at position $r_a + \epsilon$ and those that enter from region 3 start at $r_b - \epsilon$. Region 3 is a hollow cylinder with absorbing boundary at $r_b - \epsilon$ and reflecting boundary at R. Particles that enter region 3 from region 2 start at position $r_b + \epsilon$. The buffer width to prevent very short time-steps at the region boundaries is set to $\epsilon = 10$ nm. If the sampled transition time for leaving a region occurs before the next translation process selected by the Gillespie algorithm, the mRNA changes

regions and the translation state transition times are then resampled. mRNAs that first exit the nucleus are placed at position $r = R$.

Binding-competent mRNA in region 1 are unable to leave this region, because they are bound to the mitochondrion. When a binding-competent mRNA in this region loses binding competence, the mRNA is given a random radial position within $r_m < r < r_a$, with the probability of the radial position proportional to r.

Simulated mRNA have a diffusivity of 0.1 $\mu m^2/s$. This diffusivity remains constant across genes and mRNA states, consistent with experimental measurements showing little dependence of mRNA diffusivity on mRNA length [89] or number of translating ribosomes [15].

Localization measures. We use two types of localization measures, corresponding to different experimental measurements. One measure considers an mRNA localized to mitochondria if the mRNA is close enough to bind ($r_m < r < r_m + 25$ nm). This measure corresponds to experiments that chemically bind nearby mRNA to mitochondria to determine the fraction localized. The other measure considers an mRNA localized if the mRNA is close enough that with diffraction-limited imaging the mRNA appears next to the mitochondria ($r_m < r < r_m + 250$ nm). While quantitatively distinct, these measures do not lead to qualitatively different results.

Ensemble averaging. For each localization measurement shown in our results, we simulate 50 mRNA trajectories from synthesis to decay, with each trajectory having a lifetime (including time spent in the nucleus) and a fraction of that lifetime spent mitochondrially localized. The ensemble average is calculated by weighting the fraction localized of each trajectory by the trajectory lifetime,

$$f_{\mathrm{loc}} = \frac{\sum_i f_{\mathrm{loc},i} T_{\mathrm{lifetime},i}}{\sum_i T_{\mathrm{lifetime},i}} \ , \tag{14}$$

where $f_{\mathrm{loc},i}$ is the fraction of trajectory i spent mitochondrially localized and $T_{\mathrm{lifetime},i}$ is the mRNA lifetime for trajectory i. The probability that an mRNA will be included in a localization measurement, through either experimental localization measurement technique, is proportional to the lifetime of the mRNA.

Calculation of translation rates

We assume that each mRNA produces proteins at a rate k_{init}, so that the cell produces a particular protein at a rate $N_{\mathrm{mRNA}} k_{\mathrm{init}}$, where N_{mRNA} is the number of mRNA for a gene. For a steady state number of proteins, protein production must be balanced by protein decay. We assume that the primary mode of effective protein decay is cell division, such that each protein has an effective lifetime equal to a typical yeast division time of $T_{\mathrm{lifetime}} = 90$ minutes. The steady-state translation initiation rate is then taken as

$$k_{\mathrm{init}} = \frac{N_{\mathrm{prot}}/N_{\mathrm{mRNA}}}{T_{\mathrm{lifetime}}} \ . \tag{15}$$

Protein per mRNA data [22, 37] provides relative, rather than absolute, numbers for the number of proteins in a cell per mRNA of the same gene. Accordingly, we can rewrite our expression for k_{init} as,

$$k_{\mathrm{init}} = \frac{\alpha P}{T_{\mathrm{lifetime}}} \ , \tag{16}$$

where P is the protein per mRNA measurement [22, 37], and α is the proportionality constant. To calibrate, we use the gene *TIM50* as a standard, as there are available measurements of N_{prot}

= 4095 [22] and $N_{\mathrm{mRNA,TIM50}} = 6$ [23]. From Eq 15, $k_{\mathrm{init,TIM50}} = 0.1264\ \mathrm{s}^{-1}$, and with $P_{\mathrm{TIM50}} = 15.12$ and from Eq 16 gives $\alpha = 45.14$. With α and P, we estimate k_{init} across genes.

The steady-state number of ribosomes N_{ribo} on an mRNA balances ribosome addition to the mRNA at rate k_{init} and removal at rate $k_{\mathrm{elong}}N_{\mathrm{ribo}}/L$, such that $k_{\mathrm{elong}} = k_{\mathrm{init}}L/N_{\mathrm{ribo}}$. Ribosome occupancy R [38] is proportional to the ribosome density N_{ribo}/L. We can thus write,

$$\frac{k_{\mathrm{elong}}}{k_{\mathrm{elong,TIM50}}} = \frac{k_{\mathrm{init}}}{k_{\mathrm{init,TIM50}}}\frac{R_{\mathrm{TIM50}}}{R} \quad , \tag{17}$$

and apply $k_{\mathrm{elong,TIM50}} = 4$ aa/s [42] to estimate k_{elong} across genes.

Calculating MTS exposure time and mature MTS numbers per mRNA

In this section Eqs 6 and 7 are derived.

We assume MTS maturation is a Poisson process, i.e. with constant rate k_{MTS}. The probability that an MTS has not yet matured at time t after its translation is $I(t) = e^{-k_{MTS}t}$. After the MTS has been translated, the ribosome completes translation after a mean time $t_{max} = (L - l_{\mathrm{MTS}})/k_{\mathrm{elong}}$. For an MTS that matures before the ribosome terminates translation, the mean waiting time t_{wait} from MTS translation to maturity is

$$\begin{aligned}\langle t_{wait}\rangle &= \frac{\int_0^{t_{\mathrm{max}}} t\ P_{\mathrm{mature}}(t)\,\mathrm{d}t}{\int_0^{t_{\mathrm{max}}} P_{\mathrm{mature}}(t)\,\mathrm{d}t} \\ &= \frac{1}{k_{\mathrm{MTS}}}\frac{1 - e^{-k_{\mathrm{MTS}}t_{\mathrm{max}}}(k_{\mathrm{MTS}}t_{\mathrm{max}} + 1)}{1 - e^{-k_{\mathrm{MTS}}t_{\mathrm{max}}}} \quad ,\end{aligned} \tag{18}$$

where $P_{\mathrm{mature}} = k_{\mathrm{MTS}}I(t)$.

A fraction $I(t_{\mathrm{max}})$ of translated MTS regions do not mature before translation termination, so the mean time that a mature MTS is exposed on the mRNA is

$$\begin{aligned}\langle t_{\mathrm{expo,mature}}\rangle &= [1 - I(t_{\mathrm{max}})]\langle t_{\mathrm{wait}}\rangle \\ &= \frac{1}{k_{\mathrm{MTS}}}\left[1 - e^{-k_{\mathrm{MTS}}t_{\mathrm{max}}}(k_{\mathrm{MTS}}t_{\mathrm{max}} + 1)\right] \quad .\end{aligned} \tag{19}$$

The number of mature MTSs per mRNA, β_{mature}, is related to the mean number of ribosomes per mRNA codon, $\rho_{\mathrm{ribo}} = k_{\mathrm{init}}/k_{\mathrm{elong}}$. The probability that an MTS is mature at time t after ribosome initiation is $1 - I(t)$. The ribosome reaches codon x beyond its initiation point at time $t(x) = x/k_{\mathrm{elong}}$. Integrating over the codons beyond the MTS region,

$$\begin{aligned}\beta_{\mathrm{mature}} &= \int_0^{L-l_{\mathrm{MTS}}} \rho_{\mathrm{ribo}}\{1 - I[t(x)]\}\ \mathrm{d}x \\ &= \frac{k_{\mathrm{init}}}{k_{\mathrm{elong}}}\int_0^{L-l_{\mathrm{MTS}}}\left[1 - \exp\left(-\frac{k_{\mathrm{MTS}}}{k_{\mathrm{elong}}}x\right)\right]\ \mathrm{d}x \\ &= \frac{k_{\mathrm{init}}}{k_{\mathrm{elong}}}\left\{L - l_{\mathrm{MTS}} - \frac{k_{\mathrm{elong}}}{k_{\mathrm{MTS}}}\left[1 - \exp\left(-\frac{k_{\mathrm{MTS}}}{k_{\mathrm{elong}}}[L - l_{\mathrm{MTS}}]\right)\right]\right\} \quad .\end{aligned} \tag{20}$$

Supporting information

S1 Fig. Cumulative distribution of conditional and constitutive mRNA genes vs ribosome occupancy (lines indicate fraction of genes with given ribosome occupancy or less). Ribosome occupancy from Arava et al [43]. $n_{\text{conditional}} = 54$ and $n_{\text{constitutive}} = 160$. These ribosome occupancy values cover a distinct range, in comparison to those of Fig 2A, due to distinct experimental measurement techniques.
(PDF)

S2 Fig. Cumulative distribution of conditional and constitutive genes vs elongation rates (lines indicate fraction of genes with given elongation rate or less). Elongation rates calculated with data from and as described in Riba et al [42], with elongation rate equal to protein synthesis rate divided by ribosome density. $n_{\text{conditional}} = 9$ and $n_{\text{constitutive}} = 30$.
(PDF)

S3 Fig. Violin plot showing mRNA localization fraction of individual genes with instantaneous model (no maturation delay) with translation kinetics for each gene estimated from experimental data (see Methods) and 4% MVF. (A) is with mRNA diffusivity $D = 0.001\ \mu m^2/s$, (B) with $D = 0.01\ \mu m^2/s$, (C) with $D = 0.1\ \mu m^2/s$, (D) with $D = 0.2\ \mu m^2/s$, (E) with $D = 0.5\ \mu m^2/s$, and (F) with $D = 1\ \mu m^2/s$.
(PDF)

S4 Fig. Mitochondrial localization vs mitochondrial volume fraction for ATP3 for model with 40-second maturation time and with translation kinetics estimated from experimental data (see Methods). ATP3 mRNA decay time is varied, with the 600 s decay timescale used in other figures. Decay timescale has limited impact unless it is sufficiently short to compete with the timescale for a newly-synthesized mRNA to first gain binding competence.
(PDF)

S1 File. Supporting data. Data files and accompanying text files, as well as Matlab programs to create each plot.
(ZIP)

Acknowledgments

We thank T Tsuboi, M Viana, and R Subramaniam for helpful discussions and feedback on the paper.

Author Contributions

Conceptualization: Elena F. Koslover, Brian M. Zid, Aidan I. Brown.

Funding acquisition: Elena F. Koslover.

Investigation: Ximena G. Arceo, Aidan I. Brown.

Methodology: Ximena G. Arceo, Elena F. Koslover, Brian M. Zid, Aidan I. Brown.

Supervision: Brian M. Zid, Aidan I. Brown.

Writing – original draft: Ximena G. Arceo, Brian M. Zid, Aidan I. Brown.

Writing – review & editing: Ximena G. Arceo, Elena F. Koslover, Brian M. Zid, Aidan I. Brown.

References

1. Bauer NC, Doetsch PW, Corbett AH. Mechanisms regulating protein localization. Traffic. 2015; 16(10):1039–1061. https://doi.org/10.1111/tra.12310 PMID: 26172624
2. Aviram N, Schuldiner M. Targeting and translocation of proteins to the endoplasmic reticulum at a glance. Journal of cell science. 2017; 130(24):4079–4085. https://doi.org/10.1242/jcs.204396 PMID: 29246967
3. Chio US, Cho H, Shan So. Mechanisms of tail-anchored membrane protein targeting and insertion. Annual review of cell and developmental biology. 2017; 33:417–438. https://doi.org/10.1146/annurev-cellbio-100616-060839 PMID: 28992441
4. Guardia CM, De Pace R, Mattera R, Bonifacino JS. Neuronal functions of adaptor complexes involved in protein sorting. Current opinion in neurobiology. 2018; 51:103–110. https://doi.org/10.1016/j.conb.2018.02.021 PMID: 29558740
5. Wheeler RJ, Hyman AA. Controlling compartmentalization by non-membrane-bound organelles. Philosophical Transactions of the Royal Society B: Biological Sciences. 2018; 373(1747):20170193. https://doi.org/10.1098/rstb.2017.0193 PMID: 29632271
6. Maza NA, Schiesser WE, Calvert PD. An intrinsic compartmentalization code for peripheral membrane proteins in photoreceptor neurons. Journal of Cell Biology. 2019; 218(11):3753–3772. https://doi.org/10.1083/jcb.201906024 PMID: 31594805
7. Mogre SS, Brown AI, Koslover EF. Getting around the cell: physical transport in the intracellular world. Physical Biology. 2020; 17(6):061003. https://doi.org/10.1088/1478-3975/aba5e5
8. Das S, Vera M, Gandin V, Singer RH, Tutucci E. Intracellular mRNA transport and localized translation. Nature Reviews Molecular Cell Biology. 2021; 22(7):483–504. https://doi.org/10.1038/s41580-021-00356-8 PMID: 33837370
9. Biever A, Donlin-Asp PG, Schuman EM. Local translation in neuronal processes. Current Opinion in Neurobiology. 2019; 57:141–148. https://doi.org/10.1016/j.conb.2019.02.008 PMID: 30861464
10. Bramham CR. Local protein synthesis, actin dynamics, and LTP consolidation. Current opinion in neurobiology. 2008; 18(5):524–531. https://doi.org/10.1016/j.conb.2008.09.013 PMID: 18834940
11. Stephens SB, Dodd RD, Brewer JW, Lager PJ, Keene JD, Nicchitta CV. Stable ribosome binding to the endoplasmic reticulum enables compartment-specific regulation of mRNA translation. Molecular biology of the cell. 2005; 16(12):5819–5831. https://doi.org/10.1091/mbc.E05-07-0685 PMID: 16221886
12. Trcek T, Lehmann R. Germ granules in Drosophila. Traffic. 2019; 20(9):650–660. https://doi.org/10.1111/tra.12674 PMID: 31218815
13. Das S, Singer RH, Yoon YJ. The travels of mRNAs in neurons: do they know where they are going? Current opinion in neurobiology. 2019; 57:110–116. https://doi.org/10.1016/j.conb.2019.01.016 PMID: 30784978
14. Besse F, Ephrussi A. Translational control of localized mRNAs: restricting protein synthesis in space and time. Nature reviews Molecular cell biology. 2008; 9(12):971–980. https://doi.org/10.1038/nrm2548 PMID: 19023284
15. Wang C, Han B, Zhou R, Zhuang X. Real-time imaging of translation on single mRNA transcripts in live cells. Cell. 2016; 165(4):990–1001. https://doi.org/10.1016/j.cell.2016.04.040 PMID: 27153499
16. Cioni JM, Lin JQ, Holtermann AV, Koppers M, Jakobs MA, Azizi A, et al. Late endosomes act as mRNA translation platforms and sustain mitochondria in axons. Cell. 2019; 176(1-2):56–72. https://doi.org/10.1016/j.cell.2018.11.030 PMID: 30612743
17. Boengler K, Heusch G, Schulz R. Nuclear-encoded mitochondrial proteins and their role in cardioprotection. Biochimica et Biophysica Acta (BBA)-Molecular Cell Research. 2011; 1813(7):1286–1294. https://doi.org/10.1016/j.bbamcr.2011.01.009 PMID: 21255616
18. Devaux F, Lelandais G, Garcia M, Goussard S, Jacq C. Posttranscriptional control of mitochondrial biogenesis: spatio-temporal regulation of the protein import process. FEBS letters. 2010; 584(20):4273–4279. https://doi.org/10.1016/j.febslet.2010.09.030 PMID: 20875412
19. Saint-Georges Y, Garcia M, Delaveau T, Jourdren L, Le Crom S, Lemoine S, et al. Yeast mitochondrial biogenesis: a role for the PUF RNA-binding protein Puf3p in mRNA localization. PLoS One. 2008; 3(6):e2293. https://doi.org/10.1371/journal.pone.0002293 PMID: 18523582
20. Garcia M, Delaveau T, Goussard S, Jacq C. Mitochondrial presequence and open reading frame mediate asymmetric localization of messenger RNA. European Molecular Biology Organization Reports. 2010; 11(4):285–291. https://doi.org/10.1038/embor.2010.17 PMID: 20224577
21. Di Bartolomeo F, Malina C, Campbell K, Mormino M, Fuchs J, Vorontsov E, et al. Absolute yeast mitochondrial proteome quantification reveals trade-off between biosynthesis and energy generation during

diauxic shift. Proceedings of the National Academy of Sciences. 2020; 117(13):7524–7535. https://doi.org/10.1073/pnas.1918216117 PMID: 32184324

22. Morgenstern M, Stiller SB, Lübbert P, Peikert CD, Dannenmaier S, Drepper F, et al. Definition of a High-Confidence Mitochondrial Proteome at Quantitative Scale. Cell Reports. 2017; 19(13):2836–2852. https://doi.org/10.1016/j.celrep.2017.06.014 PMID: 28658629
23. Tsuboi T, Viana MP, Xu F, Yu J, Chanchani R, Arceo XG, et al. Mitochondrial volume fraction and translation duration impact mitochondrial mRNA localization and protein synthesis. eLife. 2020; 9:e57814. https://doi.org/10.7554/eLife.57814 PMID: 32762840
24. Viana MP, Brown AI, Mueller IA, Goul C, Koslover EF, Rafelski SM. Mitochondrial fission and fusion dynamics generate efficient, robust, and evenly distributed network topologies in budding yeast cells. Cell systems. 2020; 10(3):287–297. https://doi.org/10.1016/j.cels.2020.02.002 PMID: 32105618
25. Williams CC, Jan CH, Weissman JS. Targeting and plasticity of mitochondrial proteins revealed by proximity-specific ribosome profiling. Science. 2014; 346(6210):748–751. https://doi.org/10.1126/science.1257522 PMID: 25378625
26. Tsuboi T, Leff J, Zid BM. Post-transcriptional control of mitochondrial protein composition in changing environmental conditions. Biochemical Society Transactions. 2020; 48(6):2565–2578. https://doi.org/10.1042/BST20200250 PMID: 33245320
27. Saffman P, Delbrück M. Brownian motion in biological membranes. Proceedings of the National Academy of Sciences. 1975; 72(8):3111–3113. https://doi.org/10.1073/pnas.72.8.3111 PMID: 1059096
28. Berg HC, Purcell EM. Physics of chemoreception. Biophysical journal. 1977; 20(2):193–219. https://doi.org/10.1016/S0006-3495(77)85544-6 PMID: 911982
29. Reguera D, Rubi J. Kinetic equations for diffusion in the presence of entropic barriers. Physical Review E. 2001; 64(6):061106. https://doi.org/10.1103/PhysRevE.64.061106 PMID: 11736170
30. Condamin S, Bénichou O, Tejedor V, Voituriez R, Klafter J. First-passage times in complex scale-invariant media. Nature. 2007; 450(7166):77–80. https://doi.org/10.1038/nature06201 PMID: 17972880
31. Koslover EF, de la Rosa MAD, Spakowitz AJ. Theoretical and computational modeling of target-site search kinetics in vitro and in vivo. Biophysical journal. 2011; 101(4):856–865. https://doi.org/10.1016/j.bpj.2011.06.066 PMID: 21843476
32. Brown AI, Westrate LM, Koslover EF. Impact of global structure on diffusive exploration of organelle networks. Scientific reports. 2020; 10(1):1–13. https://doi.org/10.1038/s41598-020-61598-8 PMID: 32188905
33. Murugan A, Huse DA, Leibler S. Speed, dissipation, and error in kinetic proofreading. Proceedings of the National Academy of Sciences. 2012; 109(30):12034–12039. https://doi.org/10.1073/pnas.1119911109 PMID: 22786930
34. Gladrow J, Fakhri N, MacKintosh FC, Schmidt C, Broedersz C. Broken detailed balance of filament dynamics in active networks. Physical review letters. 2016; 116(24):248301. https://doi.org/10.1103/PhysRevLett.116.248301 PMID: 27367410
35. Brown AI, Sivak DA. Theory of nonequilibrium free energy transduction by molecular machines. Chemical reviews. 2019; 120(1):434–459. https://doi.org/10.1021/acs.chemrev.9b00254 PMID: 31411455
36. Fang X, Wang J. Nonequilibrium thermodynamics in cell biology: Extending equilibrium formalism to cover living systems. Annual review of biophysics. 2020; 49:227–246. https://doi.org/10.1146/annurev-biophys-121219-081656 PMID: 32375020
37. Couvillion MT, Soto IC, Shipkovenska LS Gergana & Churchman. Synchronized mitochondrial and cytosolic translation programs. Nature. 2016; 533:499–503. https://doi.org/10.1038/nature18015 PMID: 27225121
38. Zid BM, O'Shea EK. Promoter sequences direct cytoplasmic localization and translation of mRNAs during starvation in yeast. Nature. 2014; 514(7520):117–121. https://doi.org/10.1038/nature13578 PMID: 25119046
39. Bacman SR, Gammage PA, M M, Moraes CT. Manipulation of mitochondrial genes and mtDNA heteroplasmy. Methods Cell Biol. 2020; 155:441–487. https://doi.org/10.1016/bs.mcb.2019.12.004 PMID: 32183972
40. Liutkute M, Samatova E, Rodnina MV. Cotranslational folding of proteins on the ribosome. Biomolecules. 2020; 10(1):97. https://doi.org/10.3390/biom10010097
41. Bechtold B. Violin Plots for Matlab, Github Project; 2016. https://github.com/bastibe/Violinplot-Matlab.
42. Riba A, Di Nanni N, Mittal N, Arhné E, Schmidt A, Zavolan M. Protein synthesis rates and ribosome occupancies reveal determinants of translation elongation rates. Proceedings of the National Academy of Sciences. 2019; 116(30):15023–15032. https://doi.org/10.1073/pnas.1817299116 PMID: 31292258

43. Arava Y, Wang Y, Storey JD, Liu CL, Brown PO, Herschlag D. Genome-wide analysis of mRNA translation profiles in Saccharomyces cerevisiae. Proceedings of the National Academy of Sciences. 2003; 100(7):3889–3894. https://doi.org/10.1073/pnas.0635171100 PMID: 12660367

44. von Heijne G. Mitochondrial targeting sequences may form amphiphilic helices. The EMBO Journal. 1986; 5(6):1335–1342. https://doi.org/10.1002/j.1460-2075.1986.tb04364.x PMID: 3015599

45. Bykov YS, Rapaport D, Herrmann JM, Schuldiner M. Cytosolic events in the biogenesis of mitochondrial proteins. Trends in Biochemical Sciences. 2020; 45(8):650–657. https://doi.org/10.1016/j.tibs.2020.04.001 PMID: 32409196

46. Young JC, Hoogenraad NJ, Hartl FU. Molecular Chaperones Hsp90 and Hsp70 Deliver Preproteins to the Mitochondrial Import Receptor Tom70. Cell. 2003; 112(1):41–50. https://doi.org/10.1016/0092-8674(87)90660-X PMID: 12526792

47. Hoseini H, Pandey S, Jores T, Schmitt A, Franz-Wachtel M, Macek B, et al. The cytosolic cochaperone Sti1 is relevant for mitochondrial biogenesis and morphology. The FEBS Journal. 2016; 283(18):3338–3352. https://doi.org/10.1111/febs.13813 PMID: 27412066

48. Stein KC, Kriel A, Frydman J. Nascent Polypeptide Domain Topology and Elongation Rate Direct the Cotranslational Hierarchy of Hsp70 and TRiC/CCT. Molecular Cell. 2019; 75(6):1117–1130.e5. https://doi.org/10.1016/j.molcel.2019.06.036 PMID: 31400849

49. Schneider-Poetsch T, Ju J, Eyler DE, Dang Y, Bhat S, Merrick WC, et al. Inhibition of eukaryotic translation elongation by cycloheximide and lactimidomycin. Nature Chemical Biology. 2010; 6:209–217. https://doi.org/10.1038/nchembio.304 PMID: 20118940

50. Chu D, Kazana E, Bellanger N, Singh T, Tuite MF, von der Haar T. Translation elongation can control translation initiation on eukaryotic mRNAs. The EMBO Journal. 2014; 33(1):21–34. https://doi.org/10.1002/embj.201385651 PMID: 24357599

51. Kasari V, Margus T, Atkinson GC, Johansson MJ, Hauryliuk V. Ribosome profiling analysis of eEF3-depleted Saccharomyces cerevisiae. Scinetific Reports. 2019; 9 (3037). https://doi.org/10.1038/s41598-019-39403-y PMID: 30816176

52. Poulsen TM, Imai K, Frith MC, Horton P. Hallmarks of slow translation initiation revealed in mitochondrially localizing mRNA sequences. bioRxiv. 2019; p. 614255.

53. Sylvestre J, Vialette S, Corral Debrinski M, Jacq C. Long mRNAs coding for yeast mitochondrial proteins of prokaryotic origin preferentially localize to the vicinity of mitochondria. Genome Biology. 2003; 4(7):R44. https://doi.org/10.1186/gb-2003-4-7-r44 PMID: 12844360

54. Gebauer F, Hentze MW. Molecular mechanisms of translational control. Nature reviews Molecular cell biology. 2004; 5(10):827–835. https://doi.org/10.1038/nrm1488 PMID: 15459663

55. Espah Borujeni A, Salis HM. Translation initiation is controlled by RNA folding kinetics via a ribosome drafting mechanism. Journal of the American Chemical Society. 2016; 138(22):7016–7023. https://doi.org/10.1021/jacs.6b01453 PMID: 27199273

56. Backes S, Hess S, Boos F, Woellhaf MW, Gödel S, Jung M, et al. Tom70 enhances mitochondrial preprotein import efficiency by binding to internal targeting sequences. Journal of Cell Biology. 2018; 217(4):1369–1382. https://doi.org/10.1083/jcb.201708044 PMID: 29382700

57. Mukhopadhyay A, Ni L, Weiner H. A co-translational model to explain the in vivo import of proteins into HeLa cell mitochondria. Biochemical Journal. 2004; 382(1):385–392. https://doi.org/10.1042/BJ20040065 PMID: 15153070

58. Regev-Rudzki N, Yogev O, Pines O. The mitochondrial targeting sequence tilts the balance between mitochondrial and cytosolic dual localization. Journal of Cell Science. 2008; 121(14):2423–2431. https://doi.org/10.1242/jcs.029207 PMID: 18577574

59. Waltner M, Hammen PK, Weiner H. Influence of the mature portion of a precursor protein on the mitochondrial signal sequence. Journal of Biological Chemistry. 1996; 271(35):21226–21230. https://doi.org/10.1074/jbc.271.35.21226 PMID: 8702895

60. Zhao T, Chen YM, Li Y, Wang J, Chen S, Gao N, et al. Disome-seq reveals widespread ribosome collisions that promote cotranslational protein folding. Genome Biology. 2021; 22(16). https://doi.org/10.1186/s13059-020-02256-0 PMID: 33402206

61. Deshaies RJ, Koch BD, Werner-Washburne M, Craig EA, Schekman R. A subfamily of stress proteins facilitates translocation of secretory and mitochondrial precursor polypeptides. Nature. 1988; 332(6167):800–805. https://doi.org/10.1038/332800a0 PMID: 3282178

62. Eliyahu E, Lesnik C, Arava Y. The protein chaperone Ssa1 affects mRNA localization to the mitochondria. FEBS Letters. 2012; 586(1):64–69. https://doi.org/10.1016/j.febslet.2011.11.025 PMID: 22138184

63. Sharma SK, De Los Rios P, Christen P, Lustig A, Goloubinoff P. The kinetic parameters and energy cost of the Hsp70 chaperone as a polypeptide unfoldase. Nature chemical biology. 2010; 6(12):914–920. https://doi.org/10.1038/nchembio.455 PMID: 20953191

64. Banecki B, Zylicz M. Real time kinetics of the DnaK/DnaJ/GrpE molecular chaperone machine action. Journal of Biological Chemistry. 1996; 271(11):6137–6143. https://doi.org/10.1074/jbc.271.11.6137 PMID: 8626401

65. Wu S, Hong L, Wang Y, Yu J, Yang J, Yang J, et al. Kinetics of the conformational cycle of Hsp70 reveals the importance of the dynamic and heterogeneous nature of Hsp70 for its function. Proceedings of the National Academy of Sciences. 2020; 117(14):7814–7823. https://doi.org/10.1073/pnas.1914376117 PMID: 32198203

66. Gnesotto FS, Mura F, Gladrow J, Broedersz CP. Broken detailed balance and non-equilibrium dynamics in living systems: a review. Reports on Progress in Physics. 2018; 81(6):066601. https://doi.org/10.1088/1361-6633/aab3ed PMID: 29504517

67. Chia LL, McLaughlin C. The half-life of mRNA in Saccharomyces cerevisiae. Molecular and General Genetics MGG. 1979; 170(2):137–144. https://doi.org/10.1007/BF00337788 PMID: 372758

68. Chan LY, Mugler CF, Heinrich S, Vallotton P, Weis K. Non-invasive measurement of mRNA decay reveals translation initiation as the major determinant of mRNA stability. Elife. 2018; 7:e32536. https://doi.org/10.7554/eLife.32536 PMID: 30192227

69. Mishima Y, Han P, Ishibashi K, Kimura S, Iwasaki S. Ribosome slowdown triggers codon-mediated mRNA decay independently of ribosome quality control. The EMBO Journal. 2022; p. e109256. https://doi.org/10.15252/embj.2021109256 PMID: 35040509

70. MacDonald CT, Gibbs JH, Pipkin AC. Kinetics of biopolymerization on nucleic acid templates. Biopolymers: Original Research on Biomolecules. 1968; 6(1):1–25. https://doi.org/10.1002/bip.1968.360060102 PMID: 5641411

71. Duc KD, Saleem ZH, Song YS. Theoretical analysis of the distribution of isolated particles in totally asymmetric exclusion processes: Application to mRNA translation rate estimation. Physical Review E. 2018; 97(1):012106. https://doi.org/10.1103/PhysRevE.97.012106

72. Varenne S, Buc J, Lloubes R, Lazdunski C. Translation is a non-uniform process: effect of tRNA availability on the rate of elongation of nascent polypeptide chains. Journal of molecular biology. 1984; 180(3):549–576. https://doi.org/10.1016/0022-2836(84)90027-5 PMID: 6084718

73. Thanaraj T, Argos P. Ribosome-mediated translational pause and protein domain organization. Protein Science. 1996; 5(8):1594–1612. https://doi.org/10.1002/pro.5560050814 PMID: 8844849

74. Charneski CA, Hurst LD. Positively charged residues are the major determinants of ribosomal velocity. PLoS biology. 2013; 11(3):e1001508. https://doi.org/10.1371/journal.pbio.1001508 PMID: 23554576

75. Sabi R, Tuller T. Computational analysis of nascent peptides that induce ribosome stalling and their proteomic distribution in Saccharomyces cerevisiae. Rna. 2017; 23(7):983–994. https://doi.org/10.1261/rna.059188.116 PMID: 28363900

76. Elstner M, Andreoli C, Klopstock T, Meitinger T, Prokisch H. The mitochondrial proteome database: MitoP2. Methods in enzymology. 2009; 457:3–20. https://doi.org/10.1016/S0076-6879(09)05001-0 PMID: 19426859

77. Rühle T, Leister D. Assembly of F1F0-ATP synthases. Biochimica et Biophysica Acta (BBA)-Bioenergetics. 2015; 1847(9):849–860. https://doi.org/10.1016/j.bbabio.2015.02.005 PMID: 25667968

78. Gehrke S, Wu Z, Klinkenberg M, Sun Y, Auburger G, Guo S, et al. PINK1 and Parkin Control Localized Translation of Respiratory Chain Component mRNAs on Mitochondria Outer Membrane. Cell Metabolism. 2015; 21(1):95–108. https://doi.org/10.1016/j.cmet.2014.12.007 PMID: 25565208

79. Fazal FM, Han S, Parker KR, Kaewsapsak P, Xu J, Boettiger AN, et al. Atlas of Subcellular RNA Localization Revealed by APEX-Seq. Cell. 2019; 178(2):473–490.e26. https://doi.org/10.1016/j.cell.2019.05.027 PMID: 31230715

80. Zhang D, Shan So. Translation elongation regulates substrate selection by the signal recognition particle. Journal of Biological Chemistry. 2012; 287(10):7652–7660. https://doi.org/10.1074/jbc.M111.325001 PMID: 22228766

81. Zhao L, Cui Y, Fu G, Xu Z, Liao X, Zhang D. Signal Recognition Particle Suppressor Screening Reveals the Regulation of Membrane Protein Targeting by the Translation Rate. mBio. 2021; 12(1):e02373–20. https://doi.org/10.1128/mBio.02373-20 PMID: 33436432

82. Gillespie DT. Exact stochastic simulation of coupled chemical reactions. The journal of physical chemistry. 1977; 81(25):2340–2361. https://doi.org/10.1021/j100540a008

83. Gillespie DT. Stochastic simulation of chemical kinetics. Annu Rev Phys Chem. 2007; 58:35–55. https://doi.org/10.1146/annurev.physchem.58.032806.104637 PMID: 17037977

84. Mogre SS, Koslover EF. Multimodal transport and dispersion of organelles in narrow tubular cells. Physical Review E. 2018; 97(4):042402. https://doi.org/10.1103/PhysRevE.97.042402 PMID: 29758750

85. Verschoor A, Warner JR, Srivastava S, Grassucci RA, Frank J. Three-dimensional structure of the yeast ribosome. Nucleic acids research. 1998; 26(2):655–661. https://doi.org/10.1093/nar/26.2.655 PMID: 9421530

86. Dong C, Shi Z, Huang L, Zhao H, Xu Z, Lian J. Cloning and characterization of a panel of mitochondrial targeting sequences for compartmentalization engineering in Saccharomyces cerevisiae. Biotechnology and Bioengineering. 2021; 118(11):4269–4277. https://doi.org/10.1002/bit.27896 PMID: 34273106

87. Georgiades P, Allan VJ, Dickinson M, Waigh TA. Reduction of coherent artefacts in super-resolution fluorescence localisation microscopy. Journal of Microscopy. 2016; 264(3):375–383. https://doi.org/10.1111/jmi.12453 PMID: 27541861

88. Özisik MN. Heat conduction. John Wiley & Sons; 1993.

89. Calderwood A, Kopriva S, Morris RJ. Transcript abundance explains mRNA mobility data in Arabidopsis thaliana. The Plant Cell. 2016; 28(3):610–615. https://doi.org/10.1105/tpc.15.00956 PMID: 26952566